ELECTROSPUN NANOFIBERS FOR THE STUDY OF NEURAL CELL SYSTEMS

By

DAVID SILLITTI

A Thesis submitted to the

School of Graduate Studies

Rutgers, The State University of New Jersey

In partial fulfillment of the requirements

For the degree of

Master of Science

Graduate Program in Biomedical Engineering

Written under the direction of

Dr. David Shreiber

And approved by

_____

_____

_____

_____

New Brunswick, New Jersey

January 2019

ABSTRACT OF THE THESIS

ELECTROSPUN NANOFIBERS FOR THE STUDY OF NEURAL CELL SYSTEMS

By DAVID SILLITTI

Thesis Director:

Dr. David I. Shreiber

Polymer nanofibers and microfibers are an invaluable tool to biomedical research. Due to their versatility and customizability, fibers can be used to mimic various systems of the body such as the extracellular matrix and neuronal axons, and can be used to influence and study cell behavior. Electrospinning is an attractive method for generating these fibers in a high volume. Myoblasts were grown on random and aligned scaffolds of electrospun collagen nanofibers. Nanofiber anisotropy was shown to increase the fusion of myoblasts into multinucleated myotubes along the direction of the local fibers. Astrocytes cultured on electrospun Poly-L-Lactic acid nanofibers were found to have morphologies that were more similar to in-vivo astrocytes as compared to those cultured on glass. Larger nanofibers into the microfiber range were seen to induce a contact guidance effect, causing astrocytes to extend long processes along the fibers. Polymer microfibers with diameters similar to the diameter neuronal axons were used as a non-biological axon mimic which oligodendrocytes myelinate as if they were neurons. Fibers were functionalized by oxygen plasma activation and direct adsorption of Protein-A and CASPR2. Protein-A was used to bind and FC-Fusion version of CASPR2 to preserve the orientation of the protein along the fiber. Properly oriented protein increased myelination over control conditions.

Acknowledgements

This thesis represents not only my efforts, but the efforts and enthusiasm of everyone who helped me through my Masters program.

Thank you to Mom, Dad, Dan and Katie who supported me every step of the way.

Thank you Dr. Shreiber for your guidance and candid feedback and for helping me become the scientist I am today.

Thank you to Shreiber lab and all of my collaborators for the wonderful ideas, invaluable knowledge, and great memories.

Thank you to my friends for helping to keep my grounded and motivated through this whole process.

Table of Contents

Abstract……..……..……...ii

Acknowledgements……..……..……..iii

List of Figures……..……..……..……....v

Chapter 1 - Introduction……..……..……1

Chapter 2 - Astrocyte

Introduction……..……..……...5

Methods……..……..……7

Results and Discussion……..……..……..……8

Conclusion……..……..……..15

Figures……..……..……18

Chapter 3 - Oligodendrocytes

Introduction……..……..……..…...26

Methods……..……..……..……29

Results and Discussion……..……...36

Conclusion……..……..……...43

Figures……..……..……..…..45

Chapter 4 – Conclusion……..……..……....55

References……..……..……..……65

Appendix

Appendix 1 - Collagen Nanofibre anisotropy induces myotube differentiation and acetylcholine receptor clustering……..……..……52

Appendix 2 - Additional Figures for Chapter 2……..……..…63

Appendix 3 - Additional Figures for Chapter 3……..…….……64

List of Figures

Figure 2.1 - PLLA Nanofiber Electrospinning……..16

Figure 2.2 - Astrocyte Cultures on PLL Glass and PLLA nanofibers…….....18

Figure 2.3 - Non-reactive Astrocytes on Different Culture Substrates…….…...20

FIgure 2.4 - DbcAMP Treated Astrocytes on Different Culture Substrates…….…...22

Figure 3.1 - PLLA Nano- and Microfiber Electrospinning and Nanofiber SEM …..…..…41

FIgure 3.2 - Nanofiber Capture Methods ……...…….42

Figure 3.3 - Plasma Activation and Surface Adsorption of Protein-A Nanofibers…….….44

Figure 3.4 - Protein-A Concentration Affects Levels of Protein-A Adsorped ..……..…46

Figure 3.5 - OPC Adhesion to Surface Modified Dense Nanofiber Scaffolds……..….48

Figure 3.6 - Nanofiber Functionalization Affects OPC/Oligodendrocyte Interaction…….49

Figure 3.7 - Effect of Nanofiber Size on Levels of Interaction may be and Imaging Artifact……...……..……50

Figure A2.1 - Consolidated Graphs of Morphological Markers Measured in Astrocytes…….…...63

Figure A3.1 - Graphs of Additional Oligodendrocyte Cultures with Varying Microfiber Diameters……..…64

Diameters……..…64

Chapter 1 - Introduction

Nanofibers are being used to enhance our everyday lives. Air filters can be created using soy protein fibers to pull pollutants from the air [1]. Liquid nanofiltration systems employ a layer of nanofibers to entrap particles and allow fresh water to flow through [2-3]. Fibers have even been created with piezoelectric properties which can be used for myriad purposes, from nanofiber microphones to durable yarns which could harness the energy of the wearer's movements to generate electricity [4-5]. Nanofibers are a highly versatile technology due to their small scale, high surface area, and the numerous polymers and proteins which can be used to create them. In addition to these, the physical characteristics of the nanofibers can be easily customized. Fiber diameter, porosity and anisotropy can all be controlled during the fiber generation process to create a scaffold that fits the need of the user. Also contributing to their usefulness in biological research and medical applications is their similarity with the biological extracellular matrix (ECM).

The ECM is a three dimensional network of nanoscale fibrous protein structures with which cells interact to create tissues inside the body. Cells generate and secrete the components of the ECM which form into fibrils, become insoluble, and form the matrix [6] While providing structural support and spatial organization to cells and tissue, the ECM also contributes to control of the chemical environment of local tissue by balancing the local pH, regulating the levels of available growth factors, and affecting the levels of cytokines in the extracellular fluid [6-9]. The chemical and mechanical information provided by the ECM dictates cell growth, survival, migration, differentiation, and adhesion [9-10].The ECM is a vital component of every tissue in the body.

Cell interaction with the ECM is mediated by protein interactions, mechanical queues, and chemical release and signaling [9]. Cellular transmembrane proteins known as integrins bind to and interact with the proteins of the ECM, and use these binding

events to initiate and control cellular processes, such as cytoskeletal rearrangement [8], proliferation [11-12], adhesion [8, 11-12], migration [11], and others. As important as the protein composition of the matrix and binding events are the mechanical properties of the matrix. As cells in different tissues must mature differently to perform distinct functions, so too must the ECM in each tissue be different. As such, the composition of the proteins found in the ECM vary in a tissue specific manner [8-10]. By varying the protein composition, the ECM in each tissue has specific mechanical characteristics that promote the growth of that tissue [8].

Similarly, synthetic nanofibers can be customized with different physical properties, overall anisotropy, and protein functionalization to resemble the ECM, and can be used for varied biomedical purposes, such as wound dressings which incorporate nanofibers into their construction. The fibers inside of these dressings mimic the characteristics of the ECM in skin, and promote fibroblast migration and proliferation, and improves wound healing [13]. Nanofibers can also be used to grow cells for autologous grafting as well, avoiding many of the downsides of traditional grafts. When cultured on chitosan nanofibers, osteoblasts proliferate and mature into graftable bone, avoiding the pain of harvesting bone and the possibility of infection at the donor site [14-15]. Similarly, myoblasts seeded on nanofibrous scaffolds differentiate into multinucleated myotubes and may be useful for tissue engineering. [16-17].

Appended to this thesis is the paper “Collagen nanofiber anisotropy induces myotube differentiation and acetylcholine receptor clustering” by Kung et al [17], for which I contributed the electrospun collagen nanofiber culture surfaces (see Appendix 1, Methods 2.2 and Results 3.1). In the appended paper we investigated the effects of substrate alignment on myoblast differentiation into myotubes. For a cellularized musculoskeletal implant to be effective, it must 1) promote myoblast differentiation into myotubes, 2) align with the host tissue, 3) promote neuromuscular junction formation

[17]. The use of aligned culture substrates, such as polydimethylsiloxane micropatterns or poly(lactic acid) scaffolds [16], has proven effective in improving myoblast differentiation.

C2C12 myoblasts were cultured on micropatterned aligned collagen substrates and random collagen substrates. Substrate alignment increased the formation of multinucleated myotubes over the random control. Electrospun collagen nanofiber substrates provide a more biologically relevant culture substrate. Myoblasts were cultured on randomly oriented and aligned collagen nanofiber scaffolds, and myoblast differentiation, myotube alignment, and neuromuscular junction formation were investigated. Cells grown on aligned scaffolds again showed an increase in myotube formation over random scaffolds. Aligned scaffolds also induced greater formation of acetylcholine receptors, which are critical to neuromuscular junction formation. The electrospun nanofiber scaffold provided a biologically relevant substrate that may prove useful to musculoskeletal implants.

This is just one of the myriad applications of electrospun nanofibers in biological research. In this paper we will investigate how nanofibers can be used to replicate conditions found within the body, and how those systems can influence cell behavior. In chapter 2 we investigate how astrocyte morphology and reactivity are influenced by physical characteristics of their culture substrate, and in chapter 3 we protein functionalize electrospun microfibers for use as a neuron mimic with which to study oligodendrocyte myelination and multiple sclerosis.

Chapter 2 - Astrocyte reactivity in response to Polymer Nanofibers

Introduction

Astrocytes are ubiquitous glial cells which tile the entire central nervous system (CNS). In the healthy CNS, astrocytes contribute to development [18], blood flow regulation [19] and regulation of the chemical environment of the CNS [20-21]. In response to CNS injury or disease, astrocytes undergo a complex response known as astrogliosis. In the astrogliosis response, astrocytes become reactive and undergo a many changes both chemical and morphological. As astrocytes encounter the insult to the CNS and become reactive, they become hypertrophic, create additional processes, and lose their individual domains and begin to interdigitate with nearby astrocytes. Reactive astrocytes will also begin to express inflammatory and neurotoxic cytokines and proteins which will recruit nearby astrocytes to the response[22].

Astrocyte reactivity is not, however, an all or nothing response, it is a finely graded process that ranges from mild to severe [23]. Mild astrogliosis may involve only a small deviation from normal astrocyte behavior, and a return to normal activity once the insult has been resolved. On the other hand, severe astrogliosis causes drastic and possibly irreversible changes to the cells involved. Severe trauma or a breach in the blood-brain barrier can result in the formation of a compact glial scar, a collection of reactive astrocytes that creates a physical and chemical barrier to the damaged part of the CNS. Reactive astrocytes can encapsulate CNS infections [24], reseal the blood brain barrier after injury [25], and perform other beneficial functions in repairing damage to the CNS. However, reactive astrogliosis also has negative side effects; reactive astrocytes are implicated in numerous neurodegenerative diseases [23-24], prevent neuron outgrowth and reconnection after injury [26] and can encapsulate artificially implanted interventions in the brain eventually rendering them ineffective [27-29].

Improved understanding and control of astrocyte behavior, and reactive gliosis specifically, would be invaluable for improving current devices and disease treatments, and could prove useful in the generation of new treatments in the future.

During the foreign body response in the CNS, astrocytes sense and react to changes in the physical environment, such as mismatches in local stiffness [27, 30] and the local topographical landscape [31-32]. Thus, through control of the local physical environment to which astrocytes are subjected, it may be possible to predictably and beneficially affect astrocyte behavior. Previous research has showed the effect of culturing astrocytes on a nanofiber scaffold with a topography that mimics the native ECM [30-32]. These astrocytes appear less reactive as compared to astrocytes cultured on flat surfaces. In this thesis, we investigated the effect of changes in nanofiber topography on cultured astrocytes. Nanofiber scaffolds were electrospun with increasing nanofiber diameter, with the smallest fibers having diameters comparable to native ECM and the largest fibers having diameters in the near micron range.

In this thesis we measured cell hypertrophy, process extension, and cell complexity to compare the morphological changes in the astrocytes with varying nanofiber diameter. By measuring this sample of morphological changes associated with reactivity, we are able to understand some of the effects that the scaffolds have on these cells.

Methods

Electrospinning of Nanofiber mats

Dense mats of polymer nanofibers were generated by electrospinning to investigate their effects on astrocyte reactivity and morphology. Poly(L-Lactic Acid) (M_w

~260,000) was dissolved in an 80:20 mixture of dichloromethane (DCM) and dimethylformamide (DMF). Final polymer concentrations ranged from 5% w/v to 15% w/v PLLA to fabricate various size fibers. PLLA was dissolved in DCM, and left on a rocking mixer overnight to ensure a homogenous mixture. Glass coverslips (12mm circular) were taped to foil to directly collect fibers onto the glass.

Prior to electrospinning, DMF was added to the polymer mixture, and magnetically stirred for 30m. The final solution was loaded into a syringe with an 18 gauge, blunt tipped needle, placed into a syringe pump, and connected to the positive end of a voltage generator. Aluminum foil and coverslips were taped to the rotating drum of the collector, and the drum was placed between the needle and the negatively charged plate. The drum was set to rotate at a low speed (about 120 rpm) as to improve uniformity of collection but not fast enough to promote alignment of the fibers. Polymer solution was extruded at a rate of 5ml/hr, down a voltage difference of 25 kV, and collected on the rotating drum collector. To prevent fibers from floating during culture, edges of the fiber mats were secured to the coverslip using Secure Silicone Adhesive (Factor 2). A diagram of the electrospinning apparatus can be seen in Figure 2.1.

Astrocyte Isolation and Culture

Astrocytes were isolated from Postnatal day 1-2 Sprague Dawley rats, which were sacrificed and brains were collected as described in [31-32]. The meninges were removed from the brain and cortices were placed in HBSS. Brain sections were minced into small pieces and digested for 20 minutes in .1% Trypsin and .02% DNAse at 37^{o} C. Cell suspensions were then washed two times in culture media , and filtered through a 40 micron mesh. Mixed cell suspensions were then cultured at 37^{o}C in 75cm flasks with 10mL of media, with one brain per flask. Culture media was changed every 3-4 days until cells reached confluency, about 7 days. The culture media (DMEM + 10% FBS) did

not support the growth of primary dissociated neurons in culture. Confluent cultures were then placed on an orbital shaker overnight, to remove macrophages and microglia. Removal of media containing macrophages and microglia left a nearly pure astrocyte culture (as optimized by previous studies, [31-32]). Cells were harvested using .25% Trypsin/EDTA.

Reactive-like astrocytes were created through DbcAMP treatment of purified astrocyte culture. Cells were treated with DbcAMP containing media for 7-8 days, with media changes every 3 to 4 days. After treatment, reactive-like cultures were harvested in an identical manner as stated above. Harvested cells were then centrifuged at 1500 RPM for 5 minutes, and supernatant was removed. Pellet was resuspended in culture media. Astrocytes were then seeded onto nanofiber of PLL coated glass coverslips in 24 well plates, at a density of 30,000 cells per well. Cells were fixed after 24 and 48 hours of culture on the various substrates.

Immunolabeling of GFAP and Actin

Astrocytes were fixed for 10 minutes in 4% Paraformaldehyde and washed three times with PBS. Fixed cells were permeabilized with .5% Triton-X for 5 minutes, and wells were blocked with 10% Normal Goat Serum in Immunobuffer for 30 minutes. Wells were washed three times in PBS, and incubated at room temperature overnight with a 1:500 solution of Anti-GFAP polyclonal antibody produced in rabbits. The next day, the primary antibody solution was removed, cultures were washed three more times with PBS and incubated with a 1:500 dilution of AlexaFluor 568nm Conjugated Goat-anti-Rabbit secondary antibody, for 1h at room temperature. Cells were then washed three more times and incubated with a 1:100 dilution of AlexaFluor 488nm conjugated Phalloidin for 1h to label actin in the cells. After primary antibody incubation, all samples were protected from as much visible light as possible to avoid bleaching of fluorescent

labels. Coverslips with labeled cells were mounted onto glass slides using Fluorogel II Mounting Medium with DAPI. Mounted and unmounted samples were stored in a 4^{O} C cold room and protected from all visible light until imaging.

Images were acquired using an Olympus IX-81 inverted microscope with an attached Hamamatsu Orca camera and equipment was controlled with Metamorph for Olympus Basic software.

Astrocyte Counting, Area and Process Length Measurements

Image segmentation, cell counting, and process length measurements were performed manually in ImageJ version 1.50i. Average process lengths of untreated and DbcAMP treated, reactive-like astrocytes were measured from immunofluorescence images. Processes were defined as any extension longer than the body of the astrocyte. Lengths were measured starting from the edge of the cell body and traced using the ImageJ plugin NeuronJ version 1.4.3. Cells were counted from the blue channel of the RGB overlay.

Circularity calculation

Circularity for astrocytes was calculated using previously obtained area and perimeter data from manual image segmentation. Calculations were performed automatically by the ImageJ program after manual segmentation, and calculations followed [Formula 2.1], where A is the 2-D area of the astrocyte, P is the perimeter of the astrocyte, and Circ is the circularity. Circularity measures range from 1 for a perfect circle, and 0 for an infinitely elongated shape. As an astrocyte's morphology becomes more complex with more elongated processes, it's circularity will deviate further from 1.

$$Circ. = \frac{4\pi A}{P^2}$$

Formula 2.1

Statistical calculation

Statistical calculations and ANOVA tests were performed using GraphPad Prism v7.03.

Results and Discussion

Nanofiber Electrospinning

Electrospun PLLA nanofibers were generated for use as a culture scaffold. Nanofibers could be reliably generated from solutions of 6% w/v PLLA to 18% w/v PLLA. Solution concentrations below 6% were more likely to electrospray rather than generate nanofibers, while concentrations above 18% would polymerize at the needle tip and collect as large masses. Concentrations of 6%, 8%, 12%, and 15% w/v PLLA were used to generate fibers [Figure 2.1].

Increasing the polymer concentration in the solution increased the average diameter of the nanofibers in the scaffold. 6% and 8% w/v PLLA solutions produced nanofibers of average diameter 207.8±86.3nm and 442.9±234.0nm (average±standard deviation, n=43 and n=49), and were statistically similar [Figure 2.1]. 12% and 15% solutions generated scaffolds with nanofiber diameters of 1049.4±293.6nm and 1126.1±920.8nm respectively (average±standard deviation, n= 49 and n=49) [Figure 2.1]. While 12% and 15% scaffolds may have statistically similar average diameters, the 15% fibers have a much greater variance, and cells grown on these mats will interact with many different nanofiber topographies.

Astrocytes cultured on fibrous substrates exhibit in-vivo-like morphologies

The morphologies of astrocytes cultured on glass and nanofibers was observed

to investigate the effect of culture surface topography on their morphology. Astrocytes cultured on PLL coated glass coverslips exhibited a globular, rounded morphology and would form into large clusters and chains resembling structures seen in glial scars [Figure 2.2]. These astrocytes may truly be rounded, or there may be a large number of small, interlocking extensions that make the cell appear rounded. These tiny extensions have been observed in highly reactive astrocytes [33], but would not be able to be resolved in the images taken for this thesis. Cells grown on nanofibers showed a much more stellate morphology, and large, glial scar-like clusters were not observed [Figure 2.2]. These cells, which were cultured on a scaffold with a similar topography to native ECM, closely resemble astrocytes as seen in-vivo.

These findings show that nanofibers may be useful in situations where astrocytes are subjected to physical conditions that are foreign as compared to their normal experience, yet glial scarring would be a detriment. Introduction of nanofibers to these sites could provide a physical landscape similar to native ECM and possibly reduce astrocyte activation. Further investigation of these cells will be needed to determine if they are truly less reactive, as reactivity is a highly complex process.

Nanofiber Diameter Affects Astrocyte Morphology

Morphological indicators of astrocyte reactivity (hypertrophy, process extension, and increased complexity) were measured in astrocytes cultured without DbcAMP. Cell area, process length, and circularity were measured and compared within conditions across 24 and 48 hour time points. Astrocytes cultured on PLL coated glass exhibited no statistically significant change in process length or circularity, but cell area was found to decrease significantly at 48 hours [Figure 2.3]. Similar observations were recorded with smaller (6% and 8%) fibers; no difference in complexity or process length was observed, but a significant reduction in cell area was.

Astrocytes cultured on nanofibers spun from 12% PLLA solution exhibited a similar stellate morphology to astrocytes on small nanofibers, but after 48 hours cell complexity and process length increased while cell area did not decrease as it had in previous conditions [Figure 2.3]. Similarly, astrocytes cultured on the largest fibers increased in complexity and showed no reduction in cell area. However, while some long processes were seen at 48 hours, the largest fibers did not induce a statistically different increase in average process length.

As can be seen in the 12% and 15% fiber conditions, astrocytes began extending a few very long processes, which seem to follow along the length of a fiber in the culture substrate. This contact guidance effect may be present in the other nanofiber conditions, but the fiber diameters are too small to resolve in the images used in this thesis. However, the few elongated extensions were unique to the larger fibers. The effect was most pronounced in the 12% fiber condition, as evidenced by the large increase in average process length at 48 hours. The contact guidance was still present in the 15% fiber scaffold condition, but the effect was not robust enough to result in a significant increase in average process length; cell complexity increased significantly, but astrocytes extended many short processes as well. The range fiber diameter that induces this behavior may be very narrow. The effect was observed in both the 12% and 15% conditions, which have statistically similar average diameters, but the 15% solution generated scaffolds with a high variance in fiber diameter, so only some of the fibers would have been of the appropriate diameter. 12% solution generated a scaffold with much lower variance, and the elongation was more pronounced.

These results provide further evidence that astrocytes are able to detect and respond accordingly to differing physical stimuli [31-33]. By changing the weight by volume of polymer in solution used to generate the nanofibers comprising the scaffolds on which these cells were cultured, it is possible to control the behavior of these cells. As

surface roughness, stiffness, porosity, and a number of other variables possibly affected by nanofiber diameter were not investigated in this thesis, it is possible that the diameter is not the determining factor in these changes. However, these data provide evidence that through manipulation of the physical environment, astrocyte behavior can be affected. With further investigation and optimization, it may be possible to generate scaffolds which can direct astrocyte morphology in a controllable manner.

Smaller Fibers prevent morphological changes associated with reactivity

A reactive-like state was induced in the astrocytes using DbcAMP treatment. After activation, cells were cultured on nanofiber mats to study if substrate topography had an influence on astrocyte reactivity. While glial activation is a complex and heterogeneous process involving the production of specific cytokines, GFAP upregulation, and morphological changes, we investigated three morphological markers associated with astrocyte reactivity. At 48 hours, cells cultured on glass coverslips extended long processes, and significantly increased in cell area as compared to cells at the 24 hour time point. Astrocytes grown on large fibers still extended a few long processes along the length of fibers as seen in previous non-reactive cultures. Average cell area, however, did not increase between 24 and 48 hour time points on these substrates.

A different response to DbCAMP treatment was noted on smaller fibers. DbcAMP treated astrocytes cultured on 6% and 8% nanofiber scaffolds did not show a statistically significant increase in either process length or cell area. While it is difficult to ascertain if these cells are truly less reactive than cells grown on a glass substrate, they resisted the morphological changes between the 24 and 48 hour time points seen on glass. Morphologically, these cells more closely resemble non-reactive astrocytes seen in vivo.

The differing response to DbcAMP treatment based on topographical differences

is in line with previous research showing that reactive gliosis can be affected by the physical environment to which the astrocytes are subjected. By creating a culture environment that more closely mimics the native astrocyte environment, it is possible that these cells are “seeing” a topography that is helping to prevent further activation and glial scar formation, even though they have been chemically insulted.

Conclusion

Previous research has shown how astrocyte behavior and morphology can be affected by changes in their physical environment [27-32] The data presented here show similar results; by presenting the astrocytes with culture surfaces of varying nanofiber diameters, cell morphology was altered. Smaller topographical features promoted a morphology in the astrocytes that resembles those found in vivo, while larger fibers had a contact guidance effect, and induced an extension of long processes along the nanofibers of the scaffold.

However, many other physical characteristics of these scaffolds may also change with nanofiber diameter. In this thesis, we did not investigate surface roughness, porosity, or stiffness, which may also be important features to which these astrocytes are reacting. Other features, such as polymer used and surface change, may also prove valuable in directing astrocyte behavior. As further research elucidates exactly which features of these scaffolds promote these changes, it may be possible to generate nanofiber scaffolds which can predictably influence astrocyte behavior. Scaffolds combining numerous nanofiber topographies could be used to promote different responses in different areas of the culture. This type of culture could prove useful in directing the growth of axons. Glial scarring creates not only a physical barrier to neuron regrowth, but produces inflammatory cytokines and CSPGs which contribute to neuron

degeneration and prevent regrowth [22]. An optimized nanofiber system that aligns and extends astrocyte processes on one area and promotes a normal in-vivo astrocyte morphology in another would provide both a permissive environment for the growing neurons in one section while preventing neuron outgrowth in another, effectively leading the neurons to grow towards their intended targets.

Nanofiber scaffolds may also prove useful in reducing reactivity in astrocytes. As compared to DbcAMP treated astrocytes cultured on glass, those cultured on nanofiber scaffolds did not show the same morphological markers of reactivity. Smaller fibers provided the most protection, with no increase in cell area or process length. The topography of the nanofiber scaffolds is much closer to the native ECM on which these astrocytes grow, and may help resist those morphological changes. Further investigation of astrocytes should be conducted to investigate other markers of astrocyte reactivity. Reactive gliosis is a heterogeneous process, and along with morphological changes, astrocytes also produce inflammatory cytokines, CSPGs, and upregulate intermediate filaments such as GFAP and Vimentin. Understanding the changes in production of these proteins would give a more clear picture of how nanofibers affect astrocyte reactivity. Nanofibers could be used to reduce reactive gliosis in some surgical brain implants, such as Deep Brain Stimulation (DBS) Electrodes. After implantation, DBS electrodes become encapsulated in a dense glial scar which greatly reduces the effectiveness of the implant over time [27-29]. By coating the outside of the electrode with nanofibers comprised of a natural material such as collagen, it may be possible to reduce the glial scarring associated with implantation and the foreign body response, thus reducing encapsulation of these electrodes and extending their longevity.

Control of astrocyte behavior through physical queues can be achieved using electrospun nanofiber scaffolds. Many of the physical characteristics of nanofiber scaffolds can be easily manipulated, and complex structures can be created with

different physical characteristics in different areas. As it is further understood to which queues the astrocytes react, scaffolds can be optimized and fabricated to compel astrocytes to behave in a predictable manner.

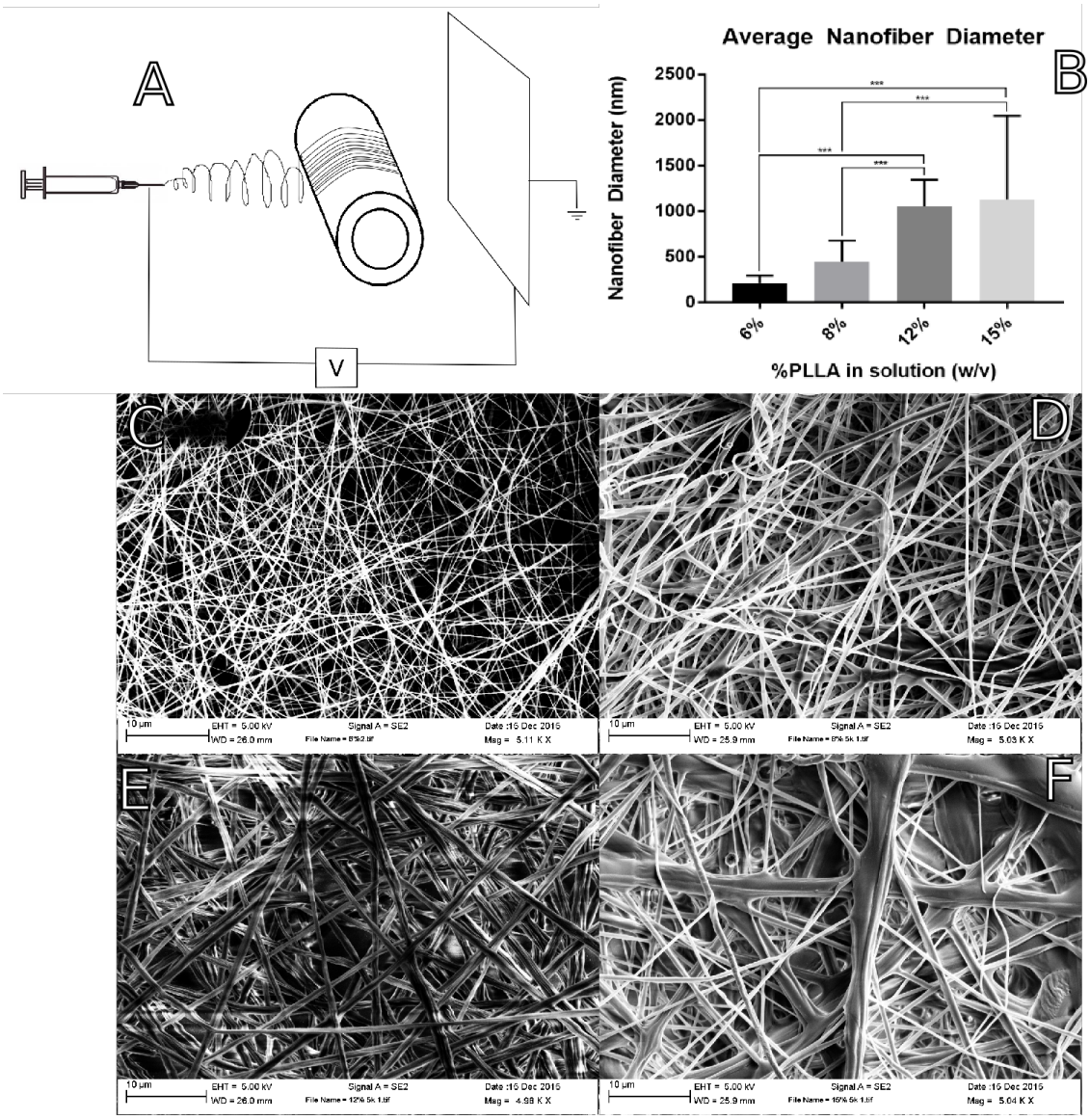

Figure 2.1 PLLA Nanofiber Electrospinning. A) Schematic of an electrospinning apparatus. A syringe loaded with the dissolved polymer solution and with an attached blunt tipped metal needle are connected to a voltage generator. The polymer solution is extruded and pulled down the voltage gradient, and the nanofibers whip in flight, and are collected on the rotating or plate collector. B) Average Nanofiber Diameters. Increasing polymer concentration increases the average diameter of the nanofibers generated. C)

Nanofiber scaffold electrospun from a 6% w/v PLLA solution. Fibers were small with low variance in diameter D) Nanofiber Scaffold electrospun from an 8% w/v PLLA solution. Fibers were statistically similar to 6% scaffolds, but had higher variance in diameter. E) Nanofiber scaffold electrospun from a 12% w/v PLLA solution. Fibers were statistically larger than previous samples. F) Nanofiber scaffold electrospun from a 15% w/v PLLA solution. FIbers generated were statistically similar to 12% mats, but with a large variance in diameter. Error bars represent standard deviation. $p<0.05$ determined by one-way analysis of variance followed by Tukey's post hoc analysis.

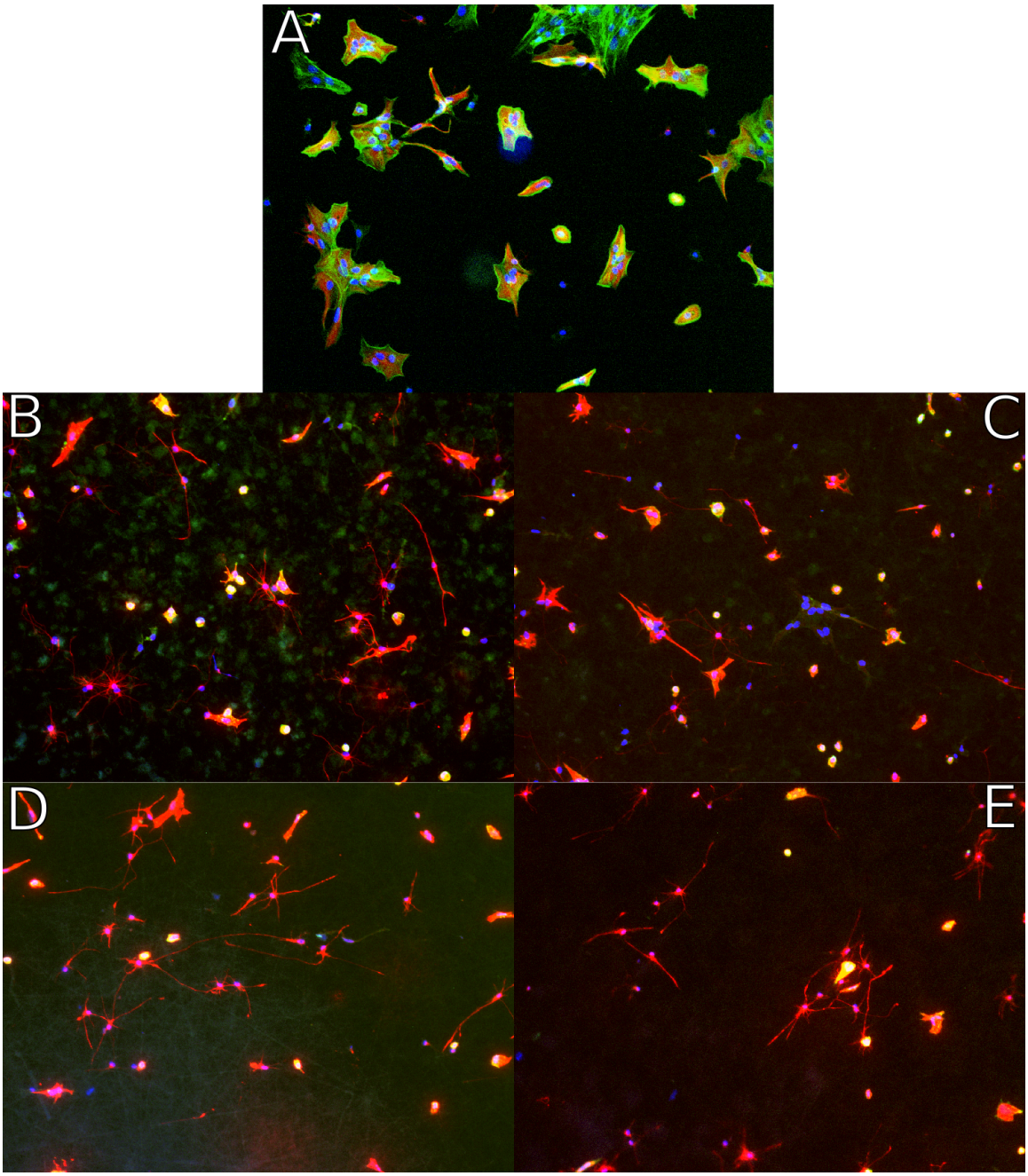

Figure 2.2 Astrocyte Cultures on PLL Glass and PLLA Nanofibers. Astrocytes cultured for 48 hours on PLL coated glass or PLLA Nanofiber scaffolds. Cells were stained against GFAP (Red) and Actin (Green) and affixed to slides with a DAPI containing mountant (Blue) A) Astrocyte culture on PLL coated glass. Astrocytes expressed a very rounded morphology and clustered together, forming scar like

groupings. B) Astrocytes cultured on a nanofibers spun from 6% w/v PLLA solution. Astrocytes expressed a much more normal in-vivo like morphology with fine processes, and appeared mostly as single cells. Scar like clusters were not observed. C) Astroctyes cultured on nanofibers spun from 8% w/v PLLA solution. Cells exhibited a similar morphology to those grown on 6% scaffolds. D) Astroctyes cultured on nanofibers spun from 12% w/v PLLA solution. Nanofibers of this scaffold were statistically larger than the previous two conditions, and astrocytes extended long processes along the fibers. E) Astroctyes cultured on nanofibers spun from 15% w/v PLLA solution. A similar morphology was expressed on these fibers as was expressed on 12% fibers.

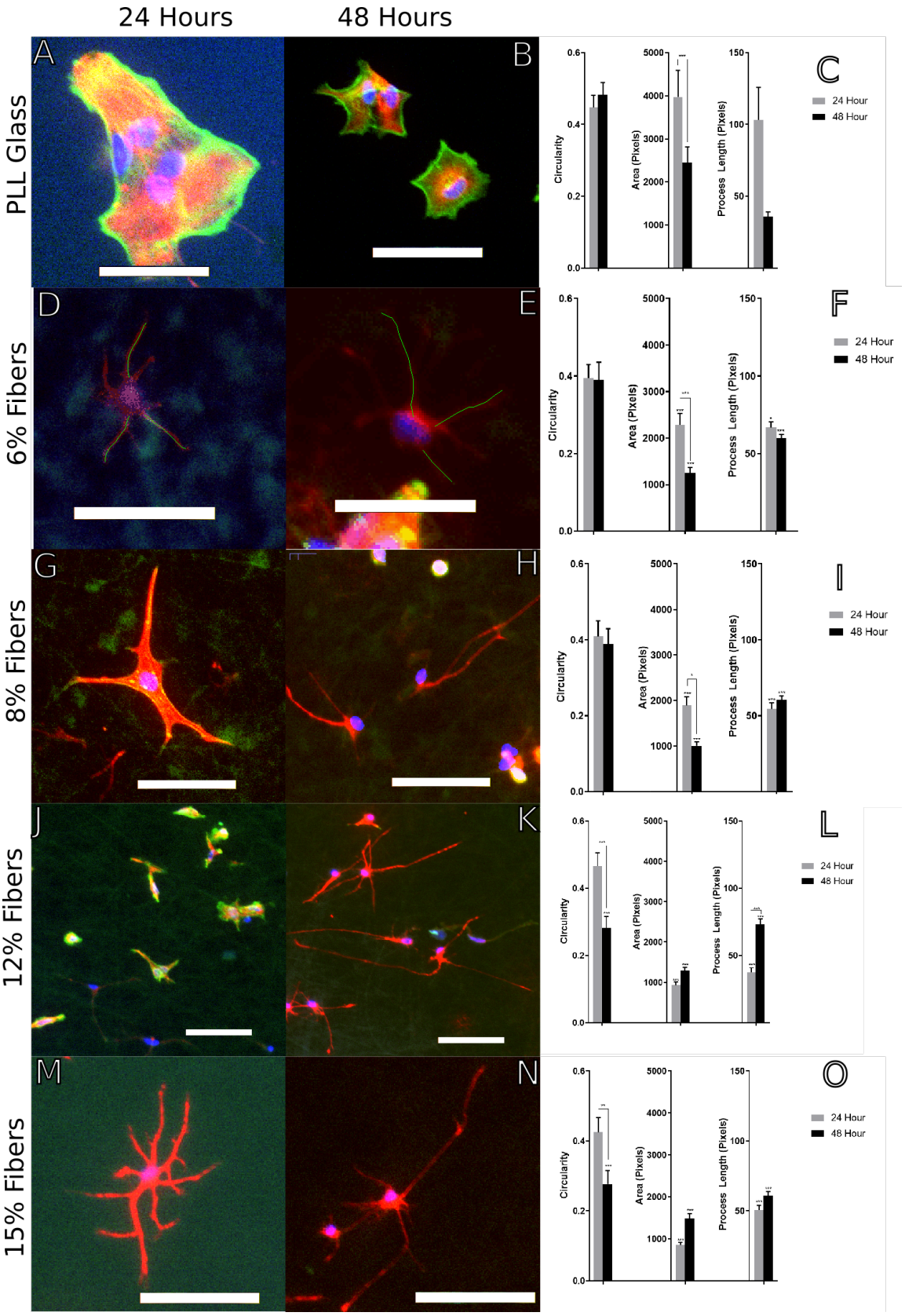

Figure 2.3 Non-reactive astrocytes on different culture substrates. Examples of

prototypical astrocytes and graphs for Circularity, Area, and Process Length. Cells were cultured on each substrate for 24 or 48 hours prior to fixing. Cells were stained against GFAP (Red) and Actin (Green) and affixed to slides with a mountant containing DAPI (Blue). A-C) Astrocytes grown on PLL coated glass coverslips showed a very rounded morphology, and clustered together. At 48 hours, astrocytes had decreased significantly in area, and the average process length decreased, albeit not statistically significantly. As the cells were highly rounded, many cells did not have measurable processes. D-I) Astrocytes grown on small diameter nanofiber scaffolds exhibited a much more “normal” astrocyte morphology with fine extensions and individual domains. At 48 hours, cell area decreased significantly, while complexity and process length remain similar. J-O) Astrocytes cultured on large diameter nanofiber scaffolds. At 48 hours in culture, cells significantly increased in complexity, and did not reduce in area as seen in other culture conditions. Cells extended long processes along the length of the nanofibers, but the effect was only pronounced enough in the 12% scaffold condition to result in an increase in average process length. Error bars represent standard error of the mean. $p<0.05$ determined by one-way analysis of variance followed by Tukey’s post hoc analysis. Asterisks over bars represent statistical difference from PLL Glass control.

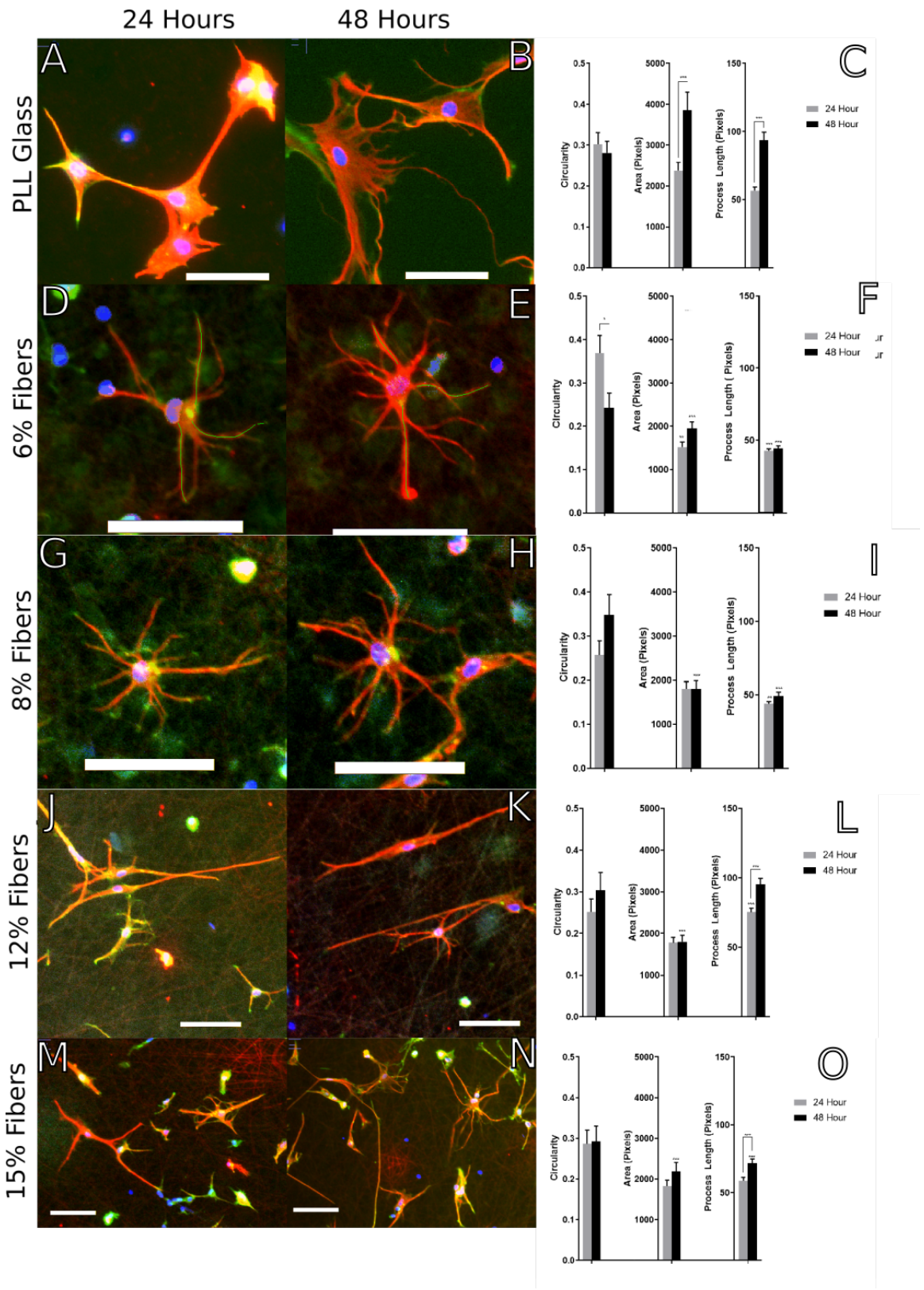
24 Hours
48 Hours
PLL Glass
6% Fibers
8% Fibers
12% Fibers
15% Fibers
A
B
C
D
E
F
G
H
I
J
K
L
M
N
O
Circularity
Area (Pixels)
Process Length (Pixels)
24 Hour
48 Hour

Figure 2.4 DbcAMP treated astrocytes. Examples of prototypical DbcAMP treated astrocytes and graphs for Circularity, Area, and Process Length. DbcAMP treated astrocytes were cultured on each substrate for 24 or 48 hours prior to fixing. Cells were stained against GFAP (Red) and Actin (Green) and affixed to slides with a mountant containing DAPI (Blue). A-C) DbcAMP

treated astrocytes grown on PLL coated glass. At 48 hours, cells appeared hypertrophic and extended processes to nearby astrocytes. DbcAMP treated astrocytes grown on 6% (D-F), 8% (G-I), 12% (J-L) and 15% (M-O) w/v PLLA nanofibers exhibited a much more stellate morphology, and scar-like clusters were not observed. All nanofiber diameters prevented the increase in cell area seen in the PLL Glass condition, and cells grown on small diameter nanofibers did not show an increase in process length. Error bars represent standard error of the mean. $p<0.05$ determined by one-way analysis of variance followed by Tukey's post hoc analysis. Asterisks over bars represent statistical difference from PLL Glass control.

Chapter 3 - Protein functionalization of electrospun nano/microfibers as a non-biological axon model for oligodendrocyte myelination

Introduction

Oligodendrocytes are glial cells found in the central nervous system that aid in neuronal signaling by providing the neurons with a myelin sheath. In the disease process of Multiple Sclerosis, myelin is progressively destroyed by the immune system [34]. Lack of myelinated neurons slows signal transduction in the central nervous system, and leads to physical disability and neuronal death. In the early stages of the disease, oligodendrocyte precursor cells (OPCs) are able to differentiate into mature oligodendrocytes and re-myelinate neurons, but this healing ability is eventually lost, and myelin sheaths continue to be destroyed [35-36]. Currently, no treatments are available to reverse the effects of Multiple Sclerosis and demyelination, only those that are capable of treating symptoms. A better understanding of the myelination process may provide insight into future treatments.

Many experiments that study oligodendrocyte myelination use in-vivo models, live neuron co-cultures, or a co-culture containing fixed neurons [35-38]. These studies provide some insight into the myelination process and treatment effectiveness, but data on the method of action can be difficult to interpret; it is hard to discern if the treatment provided changed the neurons in the culture, or affected the oligodendrocytes. Studying individual neuronal proteins is also difficult, and usually involves the use of protein knockout models [39], or case studies involving patients with mutations for proteins of interest [40]. A higher throughput experimental system with improved control could greatly accelerate pre-clinical research to both understand disease and recovery progress and test potential therapeutics.

Experiments involving OPCs cultured with paraformaldehyde fixed neurons show that the OPCs will differentiate and myelinate the neurons in the absence of live neuronal influence [38]. However, this model still introduces protein binding sites to the OPCs and oligodendrocytes, making it difficult to investigate how much of the myelination process is moderated molecularly versus physically. To the end of generating more easily interpreted data, a non-biological neuron model that provides the experimenter complete control of the physical and chemical inputs to the OPCs is needed. Electrospun nanofibers are an ideal candidate for this model. Electrospinning is a versatile and inexpensive method for generating nanofibers out of many different materials with high fiber output. Previous research has investigated oligodendrocyte interactions with fibers made from glass [41], vicryl [42], and polystyrene [43]. Research by Lee et al. [43] established that oligodendrocytes will myelinate nanofibers over 0.4μm, with peak myelination between 1.6μm to 4μm, which is similar to the diameters at which oligodendrocytes will myelinate axons in vivo [44]. These studies suggest that correct diameter of the nanofibers is sufficient for some myelination to occur, and no direct electrical or molecular input is necessary.

While the effect of nanofiber diameter on oligodendrocyte myelination has been previously studied, we now wish to reintroduce neuronal protein signals into the system. Polymer nanofibers can be functionalized with polypeptides or proteins through activation and EDC/NHS Crosslinking [45], end group functionalization [46] and direct surface adsorption. Plasma activation and protein adsorption provides a simple, inexpensive, and reliable method for non-covalently introducing proteins onto the surface of the fibers. The adsorption process leaves some of the protein in a non-functional conformation; some proteins active sites are sterically blocked and some proteins will be deactivated or denatured by the forces between the peptides and the polymer. If a neuronal protein of interest were adsorbed directly to the electrospun nanofibers prior to

culture, the segments of protein available for interaction with the oligodendrocytes would likely not be the extracellular domains with which the cells would normally interact. It is ideal to immobilize the proteins of interest using a directly adsorbed capture protein.

Of particular interest to this study is the juxtaparanodal protein Contactin-associated protein-like 2 (CASPR2), which is closely associated with myelination in the CNS. Biopsies of children with a mutation of the CNTNAP2 gene, which codes for the CASPR2 protein, showed cortical dysplasia, suggesting an effect on myelination during development [47]. In post mortem investigations of the brains of Multiple Sclerosis patients, CASPR2 is found to be missing in brain areas lacking myelination [48]. Reintroduction of this protein into the nanofiber model system should provide further insight into the function of this protein with respect to myelination.

Techniques developed by [49] allow for the synthesis of FC-Fusion CASPR2 protein, where the transmembrane and intracellular regions of the protein are replaced with human FC segments. The purified FC-CASPR2, provided generously by Dr. Davide Comolleti, or any other FC-Fusion protein, can be captured using directly adsorbed Protein-A, which specifically bind the FC region of IgG, ensuring a uniform presentation of the protein of interest to the OPCs in culture. This system will provide a versatile and simple method to investigate the contributions of individual proteins in the myelination process.

Methods

Electrospinning of Sparse nanofiber networks

To create a fiber scaffold to investigate oligodendrocyte myelination, a sparse network of fibers needed to be captured on glass. PLLA polymer solutions, glass cover slips, collectors, and electrospinning setups were prepared as previously stated in

chapter 2 of this paper [Figure 3.1]. High concentration solutions of 11% to 18% were used to generate larger fibers over the 0.4μm lower limit for myelination. Briefly, PLLA was dissolved in DCM, and left on a rocker overnight, or magnetically stirred for 3-4 hr until homogenous. DMF was then added to the solution to bring the solvent concentrations up to a 80:20 mixture of DCM:DMF. PLLA solutions were loaded into syringes with 18-gauge blunt tipped needles, and placed into the electrospinning apparatus. Syringes were connected to the positive end of the voltage generator, and pointed toward the rotating drum collector, which had previously been covered in tinfoil with 12mm circular glass coverslips. Polymer solutions were extruded at 5mL/hr down a voltage gradient of 25kV, and collected on the coverslips on the slowly rotating collector. Each sample was subjected to the fiber stream for five to ten seconds. Captured fibers were glued to glass coverslips using the secure silicone adhesive [Figure 3.2]. Fiber formation was verified using a light microscope. Randomly selected samples of fibers were sputter coated with 15nm of gold, and imaged in a Zeiss Sigma FE-SEM. SEM micrographs were used to determine the size of the fibers [Figure 3.1].

To prevent adsorption of proteins to the culture glass and to allow protein signals to be expressed only on the nanofibers of the system, a system was developed to (1) capture fibers isolated from their eventual culture surface and (2) alter these fibers while maintaining a uniform culture surface between nanofiber coating conditions. To this end, nanofibers were captured and suspended across PDMS rings [Figure 3.2]. PLLA was dissolved at concentrations from 11% w/v to 17% w/v in chloroform. Solutions were left on a rocking mixer overnight, or magnetically stirred for 3-4h until homogenous. PDMS rings with an outer diameter of 1 inch and an inner diameter of 3/4 inch were glued to tinfoil using Factor II Secure Silicone Adhesive, arranged similarly to the glass coverslips described previously. The foil and PDMS rings were taped to the rotating drum collector. Polymer solution was extruded at a rate of 5mL/h and a voltage of 25kV was used. Once

fibers were suspended across the rings, they were adhered to the rings by spreading silicone adhesive across the top of the PDMS. A razor blade was then used to free the PDMS rings, with suspended fibers, from the foil collector. Randomly selected fiber samples were glued onto 12mm glass coverslips for SEM imaging and characterization and prepared for FE-SEM imaging as described previously.

To examine oligodendrocyte adhesion on dense nanofiber networks, dense scaffolds were prepared as described in chapter 2 of this paper [Figure 3.1]. Briefly, PLLA solutions were prepared at concentrations from 11% w/v to 17% w/v in 80:20 DCM/DMF mixture. Homogenous PLLA mixtures were loaded into syringes, and loaded into an electrospinning apparatus, charged to 25kV, and extruded at 5mL/hr onto 12mm glass coverslips, which were placed on a rotating drum collector. Fiber scaffolds were secured to coverslips using Factor 2 Secure silicone adhesive [Figure 3.2], and random selections of fibers were prepared and imaged via FE-SEM to confirm fiber formation and size.

Nanofiber surface modification

To investigate effects of surface coatings and modifications on oligodendrocyte myelination, nanofibers were coated in Poly-L-Lysine (PLL), Protein-A, and CASPR2. CASPR2 and FC-CASPR2 proteins were isolated and generously donated by Dr. Davide Comeletti. Fibers were placed into 6 well plates, and fibers that were to be coated in Protein-A or CASPR2 were plasma treated, as well as plasma treatment only control samples. Samples were placed into a plasma generator and subjected to oxygen plasma, generated with 100W forward power for 2 minutes. Fibers were then treated immediately with 10µg/ml Protein-A dissolved in DiH_2O, 10µg/ml CASPR2 dissolved in DiH_2O, or pure DiH_2O, and allowed to incubate at room temperature overnight. Non plasma treated samples were treated with a solution of 50 µg/ml of PLL dissolved in

DiH_2O, or pure DiH_2O. Glass coverslips (12mm) were treated overnight with 50µg/ml PLL. After overnight treatment of each condition, nanofibers and glass coverslips were washed 3 times in PBS. Half of the Protein-A samples were then incubated for 1 hour, at room temperature, with 10µg/ml FC-CASPR2 in DiH_2O to allow the FC-CASPR2 to bind to the Protein-A on the fiber. Other samples were incubated in DiH_2O for 1 hour at room temperature. All scaffolds were washed again in PBS 3 times. To adhere the fibers to the PLL-coated coverslips, PDMS rings were then inverted over the slips. Silicone adhesive was used to secure the fibers to the edges of the coverslips, and excess fiber was cut from the rings using a razor blade, leaving modified fibers on PLL coated coverslips.

Dense and sparse nanofiber networks captured directly on glass were submitted to a similar treatment as fibers captured on PDMS rings. Scaffolds were subjected to Oxygen plasma treatment with identical parameters as stated above. Plasma treated scaffolds were then incubated overnight in 10µg/ml Protein-A, 10µg/mL CASPR2, or DiH_2O, at room temperature. Scaffolds which were not plasma treated were incubated overnight at room temperature in 50µg/mL PLL or DiH_2O. All scaffolds were washed the following day 3 times in PBS. Half of the Protein-A samples were then incubated for 1 hour at room temperature with 10µg/ml FC-CASPR2 in DiH_2O to allow Protein-A to immobilize the FC-CASPR2 to the fiber. Other samples were incubated in DiH_2O for 1 hour at room temperature. Scaffolds were then washed 3 more times in PBS.

All fiber samples, ring captured, dense, and sparse, were sterilized for 5 minutes using UV radiation in a SpectroLinker XL-1500 UV Crosslinker. Sterilized fiber mats were moved immediately to a sterile hood and used for culture the same day.

Protein-A adsorbtion effectiveness

To investigate whether or not Protein-A was adsorbed uniformly, and in a

functional orientation on the fibers, Protein-A treated fibers were incubated with fluorescent secondary antibodies. Plasma treated and non plasma treated nanofibers were incubated overnight with 10µg/ml Protein-A solution or DiH_2O. Fibers were then washed 3 times in PBS, and incubated in a 1:500 dilution of AlexaFluor 568 conjugated goat-anti-rabbit secondary antibody at room temperature for 1 hour. All samples were then washed three times in PBS, and glued to glass coverslips for imaging. All conditions used can be found in Figure 3.3.

To demonstrate that the level of protein presented on the surface of the fibers was tunable, plasma treated fibers were treated overnight with either 5µg/mL, 10µg/mL, or 20µg/mL Protein-A in DiH_2O, and treated the following day with secondary antibody. Samples were protected from visible light prior to imaging. Images were captured using Olympus IX-81 inverted fluorescent microscope with attached Hammamatsu Orca camera, and analyzed for relative fluorescent intensity using ImageJ 1.5.0 software. All pictures were captured using identical capture parameters. Nanofibers were manually segmented from each image, and the average pixel intensity was measured using the built in Measure function in ImageJ. Average background intensity was determined for each image by taking 4 square background samples from the image, and taking the average pixel intensity.

Oligodendrocyte Precursor Cell Culture

Primary Oligodendrocyte Precursor Cells (OPCs) were isolated from post-natal rat brains. Dissection of Postnatal day 1-2 Sprague Dawley rats was performed identically as described in Chapter 2 of this paper. Cerebral hemispheres were removed, freed of meninges, and minced in PBS Glucose solution. Minced tissue was digested in 10 mL PBS Glucose with .125% Trypsin and .05% DNAse for 20 minutes in a warm water bath, with shaking every 5 minutes. To stop trypsin reaction, 15 mL MEM-C was

added to the tube. The resulting suspension was then passed through a 15 micron nylon mesh, and centrifuged at 800 rpm for 10 minutes. Supernatant was removed and cells were resuspended in 10 mL of MEM-C. Mixed cell suspension was transferred to 75 cm^2 culture flasks, and cultured for 11 days, with media changes every 2-3 days.

Culture procedures and medium allow for the growth of astrocytes, microglia, OPCs, oligodendrocytes, and other cells, so it is necessary to isolate the OPCs from the mixed culture. At day 11, flasks were placed on a radial shaker inside of an incubator for 1 hour and 30 minutes at 260 rpm to remove loosely adherent microglia. The supernatant was removed, and replaced with 10mL of fresh MEM-C. Flasks were placed back onto the shaker and left shaking at 260 rpm overnight to remove OPCs from the culture surface. The next day, supernatant was removed and passed through a 15μm nylon mesh, which is only large enough to pass single cells, thereby removing the majority of astrocytes, which tend to clump together. Filtered supernatant was centrifuged at 1200 rpm and resuspended in 10mL N2B2 media. Supernatant was placed into a petri dish and replaced into an incubator for 10 minutes. Since microglia will more readily attach to the dish then OPCs, this step will further remove any impurities in the culture. After 10 minutes, the supernatant was poured into a conical tube, and the dish was lightly washed with 10mL more of N2B2 media to further remove loosely adherent OPCs. The cell suspension was once again centrifuged at 1200rpm for 5 minutes, supernatant was removed, and the pellet was resuspended in 5mL N2S media. The final cell suspension was placed into a 75cm^2 culture flask, with a PLL coated bottom surface. Purified OPC cultures were allowed to grow for at least 2 days prior to harvest and experimentation, with media changes every 2-3 days as necessary.

Immunolabeling of Myelin Basic Protein and Platelet Derived Growth Factor Receptor - α

On day 12 of culture, cells were fixed in 4% PFA for 5 minutes and washed in PBS 3 times. Cells were permeabilized for 5 minutes with .5% Triton-X in PBS, and wells were blocked in 10% normal goat serum (NGS) in immunobuffer for 30 minutes. After blocking, NGS was removed and cells were incubated with a mixture of 1:500 Rat Anti-MBP and 1:500 rabbit anti-PDGFR-α primary antibodies overnight at room temperature. The next morning, primary antibody mixtures were removed and wells were washed 3 times in PBS. Cells were treated with 1:500 AlexaFluor 568 conjugated Goat-anti-Rabbit secondary antibody for 1 hour at room temperature to label PDGFR-α. After 1 hour, secondary antibody solutions were suctioned out, wells were washed 3 times in PBS, and a solution of 1:500 Alexafluor 488 conjugated Goat-Anti-Rat secondary antibody was added to each well for 1 hour. After incubation at room temperature, scaffolds were once again washed 3 times in PBS, and incubated for 10 minutes with 1:10000 dilution of DAPI before 3 final washes. All samples were protected from as much visible light as possible during all staining and washing steps. Triple labeled cells were stored in 24 well plates in PBS, or were mounted to glass slides using Fluorogel-II mounting medium with DAPI. All samples were stored in a $4C^{O}$ cold room and protected from light until imaging

Statistical Calculations

Statistical calculations and ANOVA tests were performed using GraphPad Prism v7.03, and chi square tests were performed in LibreOffice Calc Version 5.0.1.3.

Results and Discussion

Nanofiber Electrospinning

Two different solvent conditions were employed in this paper to dissolve the PLLA

for electrospinning; a DCM/DMF mixture, and chloroform. While fibers could be generated with either, the different solvents had a large influence on the fibers that were generated. Fibers spun from a solvent mixture of DCM/DMF were able to be spun directly onto glass coverslips, and generated fibers from polymer concentrations of 6% to 18% w/v PLLA. Concentrations below 6% were more likely to electrospray than generate fibers, while mixtures above 18% would solidify at the needle tip, and collect as large masses, rather than being pulled toward the collector. Concentrations between 6% and 18% performed as expected, with fine fibers showing the characteristic whipping motion while in flight.

Since these fibers were collected directly onto glass, any surface modifications that were performed on the fibers were also performed on the glass, resulting in proteins being presented on the culture surface, instead of only on the nanofiber axon models. To prevent protein presentation on the glass substrate, a number of methods were attempted to introduce functional Protein-A selectively to the fibers. Since Protein-A binds to FC-segments of IgG antibodies, Functionalization was assessed by treating the fibers with fluorescent IgG secondary antibodies, which bind to Protein-A with high affinity, and measuring changes in fluorescent intensity of the nanofibers with a fluorescent microscope. Three methodologies were investigated for selective Protein-A functionalization: direct addition of Protein-A to the polymer solution, emulsion electrospinning, and capture of nanofibers separated from the culture surface.

Direct addition of the protein to the polymer solution resulted in no fluorescent intensity increase over the control fibers (Data not shown), likely due to protein denaturation either by the solvents or the strong electric field to which the fibers are subjected during electrospinning.

Emulsion electrospinning produced similarly dissatisfactory results. To generate an emulsion for electrospinning, SDS and Protein-A were added to Deionized water to

create the water phase. This phase was added to the DCM/DMF/polymer solution under vortex to induce an emulsion. Once spun, treated with fluorescent antibody, and visualized, small clusters of bright fluorescence were observed across the fibers (data not shown). However, upon repeated trials, emulsion electrospinning was found to be an unreliable method for protein introduction; In numerous repeated attempts to spin these fibers, no increase in fiber fluorescence was observed again.

To capture the nanofibers in such a way that they could be modified and later applied to glass coverslips, nanofibers were captured across PDMS rings. When placed on a rotating collector, and subjected to the nanofiber stream, the fibers would be captured suspended across the void in the ring, and the fibers could be secured to the ring using a silicone glue. This allowed for the fibers to be easily transported and to have various surface treatments applied. Fibers were then able to be glued back onto PLL treated glass coverslips, giving a uniform culture surface regardless of nanofiber surface coating.

When DCM/DMF fibers were spun across the PDMS rings, the fibers were not captured suspended across the rings, but instead made contact with the tinfoil inside of the ring. When the fibers contacted the foil inside of the ring, they were too loose to later attach to the glass coverslips after surface modification, and could not be used. A different solvent was needed to generate fibers which would behave appropriately with the PDMS rings.

When chloroform was used as the solvent, much larger fibers were spun. Chloroform fiber diameters ranged from about 4μm to about 12 microns, and were able to be easily captured across PDMS rings. This was most likely due to the lack of the fibers whipping while in flight. While the chloroform/PLLA mixture still exhibited the Taylor cone, the fibers appeared to deposit in a straight line. The lack of random whipping can also be seen in the highly aligned nature of these fibers, as compared to

those spun from DCM/DMF. Fibers were likely pulled across the gap in the ring by the ring walls, while whipping fibers would continue onto the tin foil. Concentrations from 11% to 17% w/v PLLA were used to generate the fibers.

Nanofiber functionalization with surface adsorbed proteins

To ensure that Protein-A was being adsorbed in a functional conformation, Protein treated fibers and controls were incubated with fluorescent secondary antibodies. If Protein-A was present and functional, then Protein-A would bind and immobilize the secondary antibody, and the fibers would have a high fluorescent intensity under a fluorescent microscope. As stated previously, this methodology was applied to each attempted method of generating protein-A coated nanofibers; direct protein addition, emulsion electrospinning, and adsorption. Oxygen plasma treated fibers with adsorbed Protein-A were the only fibers found to exhibit an increase in fluorescence [Figure 3.3].

Only the two fiber conditions treated with both Protein-A and secondary antibody showed an appreciable increase in fluorescence over control fibers. Of these two sets, only fibers that were treated with plasma, Protein-A, and secondary antibody showed a statistically significant increase in intensity over the control conditions; while it is possible to adsorb Protein-A directly to the fibers without plasma activation, it is much less efficient.

Interestingly, as evidenced by the Plasma+ Protein- Secondary+ condition, it does not appear that secondary antibodies adhere to the plasma treated fibers, or if they do adhere, they are no longer fluorescent. As such, it is safe to assume that any fluorescence present in these experiments is due to the adsorption of Protein-A and subsequent binding of the FC portion of the fluorescent secondary antibody.

Next, we wished to investigate whether the amount of Protein-A adsorbed to the nanofibers could be regulated. Plasma treated fibers were incubated with varying

concentrations of Protein-A solutions prior to treatment with secondary antibody. All protein treated fibers exhibited an increase in fluorescent intensity over the control, and a significant intensity increase was seen as the concentration of Protein-A was increased from 5µg/mL to 10 ug/mL to 20µg/ml. While the increase in fluorescent intensity from 10µg/ml to 20 ug/ml was only 450 units, the increase in Protein-A adsorption is likely more pronounced than the images were able to capture. At the exposure time of 1300ms needed to reliably locate fibers in the control conditions, many of the pixels in the 20µg/ml fibers were at the maximum sensor intensity of 4095 units. Protein-A can be captured reliably in a functional orientation using plasma activation, and direct adsorption, and further used to immobilize other proteins to the fibers.

OPC/Oligodendrocyte Adhesion to Dense Nanofiber Scaffolds

Oligodendrocytes and Precursor cells were cultured on dense, surface modified nanofiber scaffolds to investigate the modifications' effects on cellular adhesion. Cell nuclei, stained with DAPI, were counted in 18 3.840mm^2 fluorescent micrographs for each condition. Untreated control scaffolds presented an average of 5±0.129 cells per image. Treating the scaffolds with either PLL or oxygen plasma resulted in a statistically insignificant increase to 8.278±0.310 and 8.278±0.203 average cells per image respectively (Figure 3.5). After plasma treatment, adsorption of Protein-A did not significantly increase cell adhesion over plasma treatment alone. Adsorped CASPR2 protein, however, increased the average cells per image significantly to 19.44±.566.

The addition of CASPR2 increased the ability of the oligodendrocytes and OPCs to adhere to the nanofibers. As the addition of Protein-A did not significantly increase the amount of adhered cells, the addition of protein alone is not enough to encourage cell interaction with the surface; the adsorped protein must have a specific interaction with the cell of interest. CASPR2 increased cell adhesion above the levels seen in PLL

coated conditions, a coating which has been used in previous studies to promote oligodendrocyte interaction with and wrapping of nanofibers.

Cells were also stained for MBP and PDGFR-α to investigate if the morphology of the cells was measurably different between conditions. However, after culturing, cells did not spread on any of the surfaces, and the morphology was not measurable.

Nanofiber Myelination

OPCs were cultured with surface modified nanofibers, and the percentage of fibers with at least one myelinated segment was recorded. Surface modifications were PLL coated, no coating, plasma treated, Protein-A coated, CASPR2 coated, and FC-CASPR2 coated nanofibers. The percentage of myelinated fibers was used as a metric for discerning which modifications increased cell interaction with the fibers. Statistical significance was determined using a chi square test between conditions. Percent of myelinated fibers in each condition was compared to the percent of myelinated fibers in the PLL coated condition.

In preliminary cultures, surface modifications mostly promoted lower cell interaction with the fibers with respect to the levels of interaction recorded in PLL coated fiber conditions [Appendix 3]. At best, nanofibers treated with Protein-A and CASPR2 provided levels of interaction statistically similar to those seen in PLL coated fibers. A final culture was performed with all of the available modification conditions. In this culture, all conditions investigated previously performed as expected, providing fewer myelinated nanofibers than PLL coated fibers. FC-CASPR2, however, induced more interaction than even the PLL coated condition.

Oligodendrocytes will interact with these polymer fibers regardless of the surface properties of the fibers. However, having appropriate surface coatings greatly increases the rate at which the cells will interact. Coating the fibers with a standard cell culture

surface coating promotes a higher level of interaction than just the unmodified PLLA fibers themselves. Addition of relevant binding proteins, and conservation of the biological orientation of the domains of those proteins promotes a level of interaction that is comparable to or higher than levels seen in PLL. This nanofiber system with adsorbed proteins allows for a more biologically relevant neuron mimic than previously studied.

Increasing Fiber Diameter may increase myelination

In PLL, No coating, Protein-A, and CASPR2 conditions, the number of fibers with myelination increase with increasing fiber diameter [Figure 3.7]. This is consistent with the finding that in brain development, larger axons are myelinated prior to smaller axons [44], and the finding that oligodendrocytes preferentially myelinate nanofibers over a critical diameter [43-44].

In these microfiber-OPC co cultures, this increase may be due to increased surface area, which allows for an increased chance of interaction between the cells and the nanofibers, or due to the cells' natural proclivity to myelinate larger axons or nanofibers. However, when imaged at a high magnification, it was observed that some cells that appeared to be wrapping fibers were actually extending processes along the fiber, or growing on the glass substrate underneath the fibers [Figure 3.7]. At lower magnifications, these cells are indistinguishable from apparently myelinated fibers. The larger fibers may act as a culture substrate for the oligodendrocytes, which may attach and grow on the fibers without actually wrapping them. The larger fibers also increase the likelihood that a cell adhered to the glass underneath the fibers will be visible through the fiber, and appear to be interacting when it is not. Further research is required to understand if this apparent diameter dependence is actually present, or a manifestation of these imaging artifacts. Transmission Electron Microscopy (TEM) would be an effective means of determining if cells are wrapping fibers, or simply growing along

them.

Conclusion

Electrospun nanofibers have been used previously to study aspects of oligodendrocyte function and myelination [41-43]. While the impact of the physical characteristics of the fibers have been investigated modification of the surface of the nanofibers provides more insight into the process of myelination. While it has been shown that oligodendrocytes respond to the diameter of axons, and preferentially myelinate those above a critical size, the myelination process involves many more inputs to drive myelination to completion.

Protein signals to myelination have previously been studied using in vivo models or case studies [39-40, 47-48]. With a non-biological model, it is possible to introduce single proteins onto a system with a previously measured level of myelination, and observe changes in nanofiber myelination. Through an indirect immobilization of FC-Fusion proteins of interest using directly adsorbed Protein-A, it is possible to present these proteins in a uniform orientation, increasing the biological relevance of this model. By introducing proteins back into a controlled non-biological axon model, research into the effects of individual proteins on myelination will be more straightforward.

The juxtaparanodal protein CASPR-2 has been previously implied to be crucial to the myelination process [47-48]. These experiments supply further evidence for this theory. Introduction of CASPR2 onto electrospun nanofibers induced a level of interaction, as measured by percentage of myelinated fibers, that was on par with a coating of PLL. As the protein was directly adsorped following oxygen plasma treatment, CASPR2 was oriented randomly, with no means of controlling what domain of the protein, if any, would be available for cellular interaction. Still, some of the protein must

have been immobilized in a relevant orientation, given the increase in myelination. By introducing orientation uniformity through indirect capture of FC-CASPR2, Oligodendrocytes myelinated at a higher rate than those cultured with PLL coated fibers or with directly adsorbed CASPR-2.

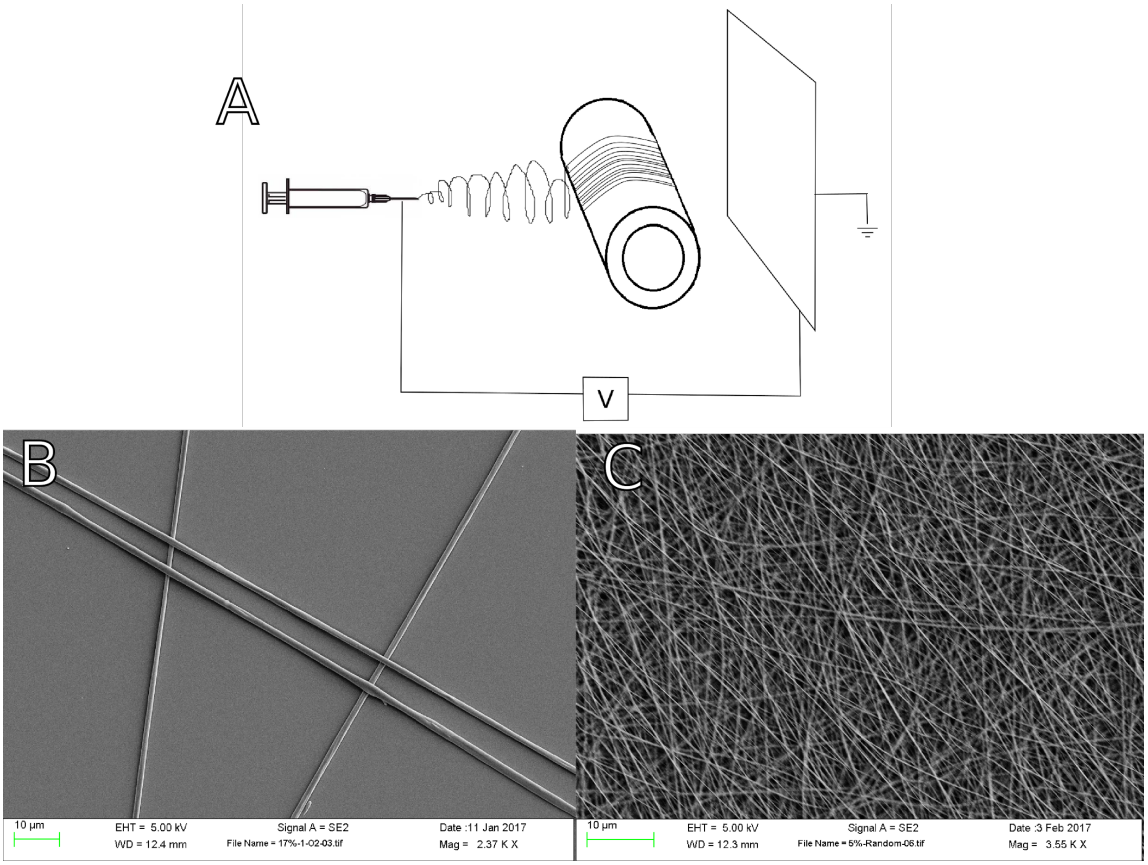

Figure 3.1 Nanofiber electrospinning set-up and nanofiber SEM. A) A diagram of an electrospinning apparatus. To generate nanofibers, the polymer solution is loaded into a syringe with a blunt tipped metal needle and connected to a voltage generator. The opposing end of the voltage generator is connected to a grounded metal plate. The voltage is applied as the polymer is extruded and fibers fly from the needle to the grounded plate and collected on a rotating mandrel. B) Sparse nanofiber scaffolds were created by exposing glass coverslips or PDMS rings to the fiber stream for 5-20 seconds. C) Dense nanofiber scaffolds were collected by subjecting glass coverslips to the fiber stream until fully coated in fibers.

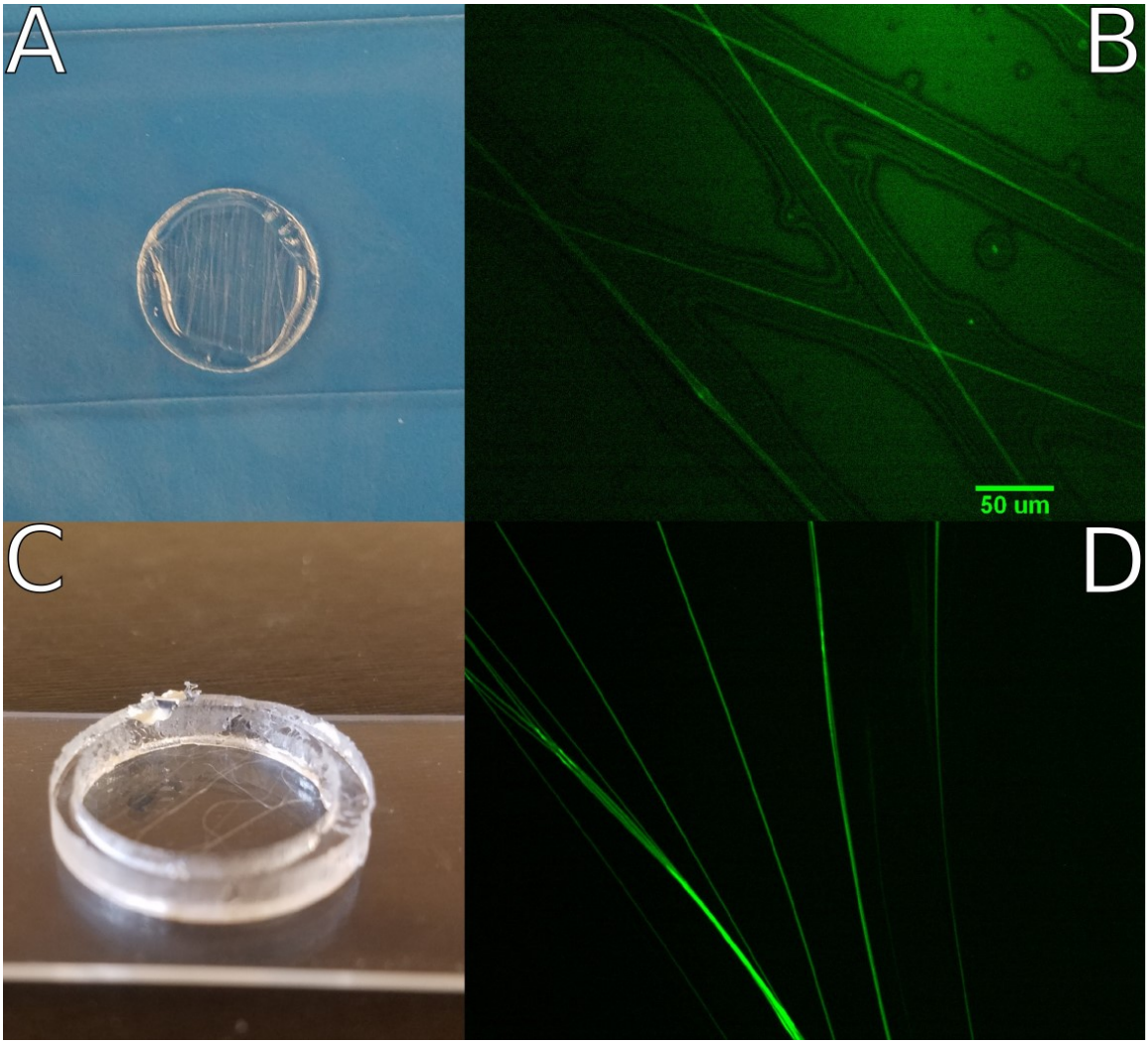

Figure 3.2 Nanofiber capture methods. A) Nanofibers were captured directly on and glued to glass coverslips which were later used for cell culture. B) When nanofibers were captured directly on glass coverslips, plasma activated, and modified with Protein-A, proteins were bound to both the fibers and the glass. Samples were plasma treated and incubated with Protein-A in DiH2O. Protein-A was visualized by incubation with a fluorescent secondary antibody. C) Polymer nanofibers were captured across PDMS rings to separate the nanofibers from the eventual culture surface. D) Nanofibers treated with plasma, Protein-A, and fluorescent secondary antibody as seen in B), but then

glued back on to unmodified glass cover slips. Background fluorescence was greatly diminished, indicating that protein expression was selective to the nanofibers.

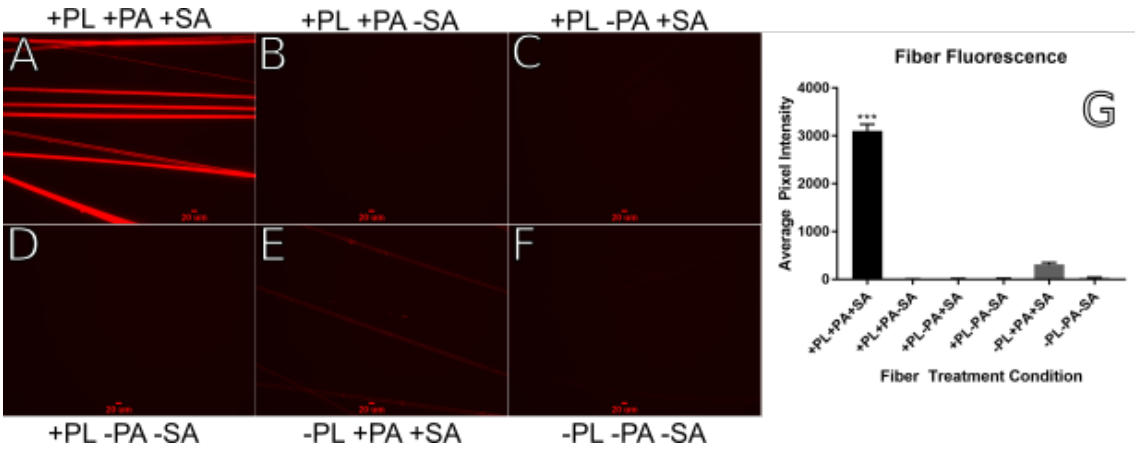

Figure 3.3 Plasma activation and surface adsorption of Protein-A to nanofibers. Nanofibers were subjected to combinations of Plasma activation, incubation with Protein-A, and incubation with fluorescent secondary antibody. A) Fluorescent image of nanofibers which were plasma treated, incubated with Protein-A, followed by fluorescent antibody (n=20 fibers). B) Nanofibers which were plasma treated, and incubated with Protein-A (n=13 fibers). C) Nanofibers which were plasma treated, and incubated with fluorescent antibody (n=19 fibers) D) Nanofibers which were plasma treated only (n=15 fibers). E) Nanofibers incubated with Protein-A and fluorescent secondary antibody (n=15 fibers) F) Control fibers with no surface modifications (n=14 fibers). G) Fluorescent intensity of nanofibers with varying modifications. Fibers were manually segmented and average pixel intensities for each fiber were determined. Background intensities were calculated by taking 4 square samples of the image background with no fibers present. Average background pixel intensities were subtracted from the average fiber intensities for each image. Only conditions with both Protein-A and fluorescent secondary antibody were found to have any appreciable increase in intensity, and only fibers treated with all three variables showed a statistically significant increase. Error bars represent standard error of the mean. $p<0.05$ determined by one-way analysis of

variance followed by Tukey's post hoc analysis.

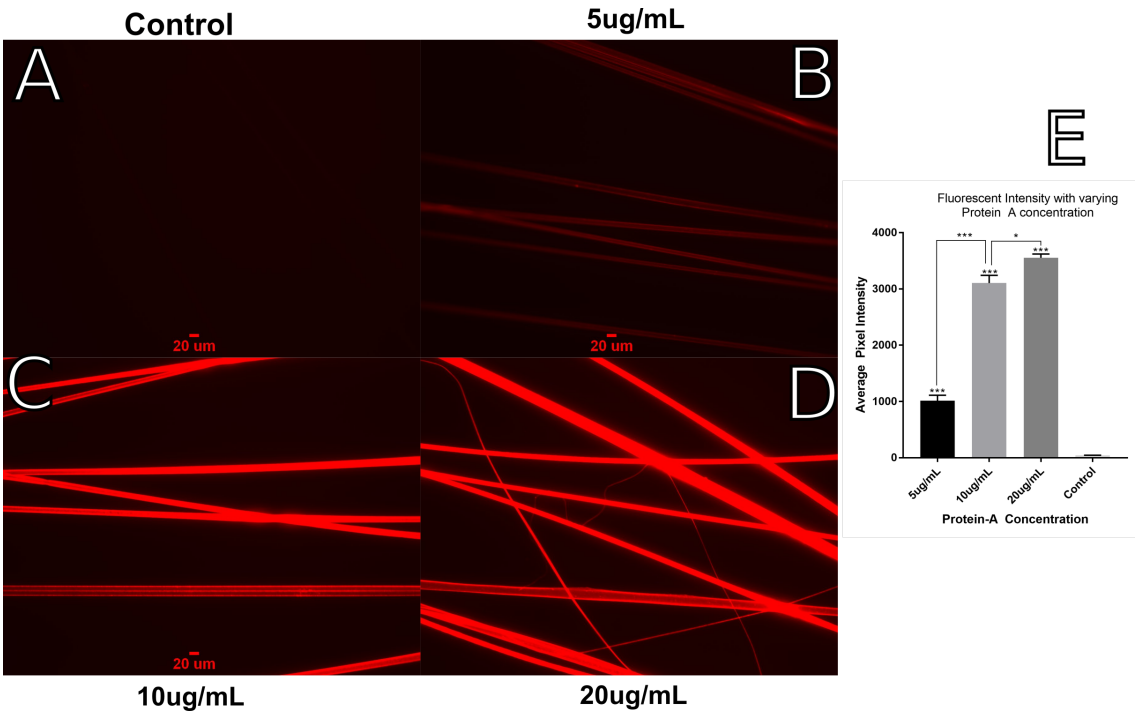

Figure 3.4 Protein-A concentration affects levels of Protein-A adsorbed on fibers. Polymer nanofibers captured across PDMS rings were plasma activated and treated with various concentrations of Protein-A in DiH2O before incubation with a fluorescent secondary antibody. A) A control condition where fibers were treated with pure water instead of a Protein-A solution (n = 14 fibers). B) Nanofibers treated with 5 µg/mL Protein-A solution (n=21 fibers). C) Nanofibers treated with 10 µg/mL Protein-A solution (n = 17 fibers). D) Nanofibers treated with 20 µg/mL Protein-A solution (n = 17 fibers). E) Fluorescent intensity with varying Protein-A concentrations. Nanofibers were manually segmented from background, and an average pixel intensity for each fiber was determined. Background from each image was calculated by taking 4 square samples of background with no nanofibers present, and finding the average pixel intensity. Individual image background values were subtracted from the average intensity of each nanofiber. Average intensity was seen to increase with increasing Protein-A

concentrations. Error bars represent standard error of the mean. $p>0.05$ determined by one-way analysis of variance and Tukey's post-hoc analysis

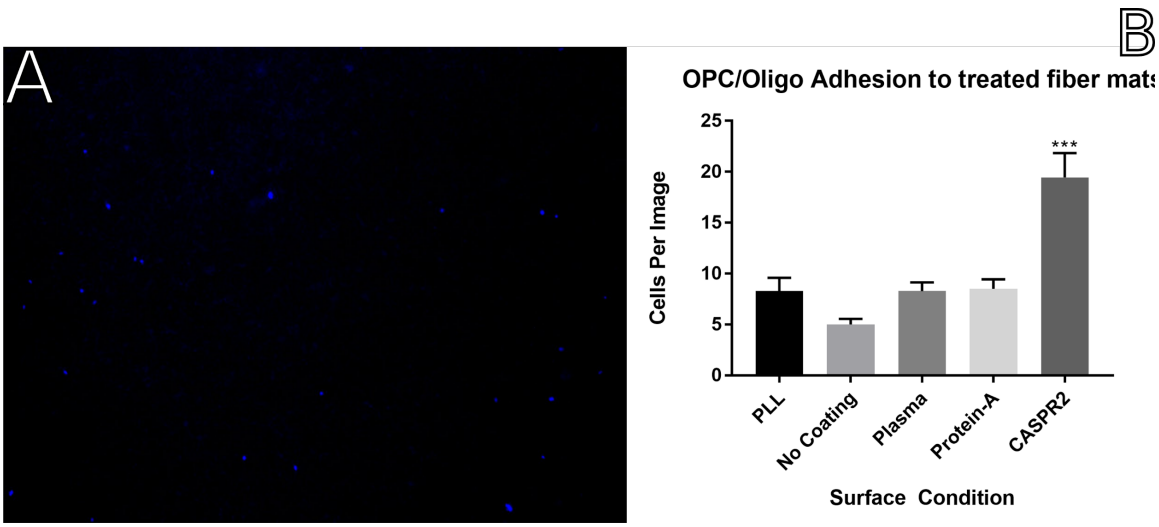

Figure 3.5 OPC adhesion to surface modified dense nanofiber scaffolds. A) Dense nanofiber scaffolds were manufactured and glued to glass coverslips. Scaffolds were functionalized by plasma activation, Protein-A coating or CASPR2 coating. PLL coated and non-functionalized fibers were used as controls. OPCs were cultured, fixed, and stained on the scaffolds, and the average number of cells per image was tabulated. B) OPC/Oligo adhesion to treated nanofiber mats. Cell nuclei were manually counted from 18 images from each condition. A statistically significant increase in cells per image was observed only on scaffolds treated with CASPR2. Error bars represent standard error of the mean. $p>0.05$ determined by one-way analysis of variance and Tukey's post-hoc analysis.

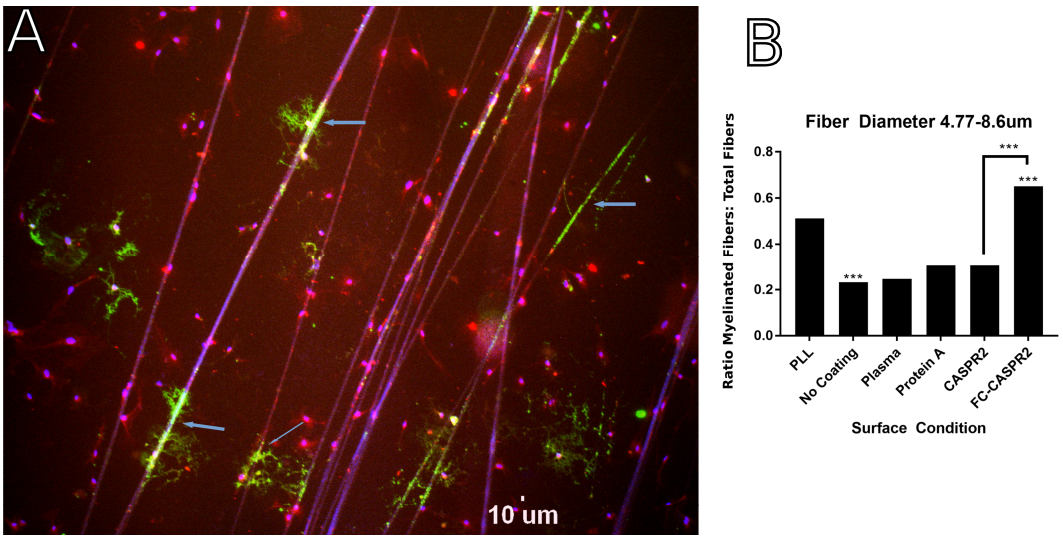

Figure 3.6 Nanofiber functionalization affects OPC/Oligodendrocyte interaction. A) Sparse microfiber scaffolds were functionalized via plasma activation, Protein-A coating, CASPR2 coating, or Protein-A immobilized FC-CASPR2 coating. Non-functionalized and PLL coated fibers were used as controls. Cells were stained for MBP (Green), PDGRF-α (Red) and DAPI (Blue). Arrows indicate where MBP+ oligodendrocytes are interacting with microfibers. B) Percent myelinated fibers with different microfiber functionalization. Total fibers and fibers with at least one myelinated segment were counted manually. Only cultures containing fibers treated with CASPR2 presented in a uniform orientation showed an increase in cell interaction over the PLL control condition. Protein-A immobilization of FC-CASPR2 increased interaction over levels seen in directly adsorped CASPR2. $p>0.05$ determined by chi square analysis between functionalization conditions.

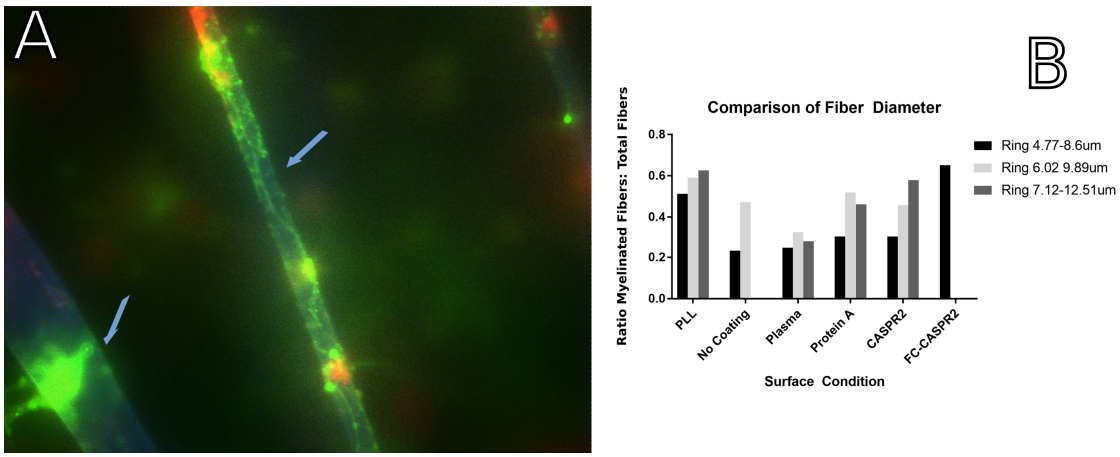

Figure 3.7 Effect of nanofiber size on levels of interaction may be an imaging artifact. A) High magnification images of fibers (7.12-12-15 μm diameter) and cells (Green = MBP, Red = PDGFR-α, Blue = DAPI). Arrows indicate an oligodendrocyte that has extended processes along the length of the fiber instead of wrapping around the fiber (1) and an MBP+ oligodendrocyte visible through the fiber, but not interacting with that fiber (2). At lower magnification, these cells appear to be wrapping the fibers. B) Cell interaction with fibers increases with increasing fiber diameter. Total fibers and myelinated fibers were manually counted for three separate cultures, and the percent of myelinated fibers for each condition were compared. Interaction was generally found to increase with increasing diameter.

Chapter 4 - Conclusion

The physical conditions that a cell experiences can affect cell behavior as much as chemical signals. Manipulation of the physical environment can be used to influence or direct cell behavior. Nanofibers provide a valuable platform with which to engineer cell activity both due to their similarity to natural ECM and customizability. This thesis provides further evidence of how manipulation of the physical environment, particularly with electrospun nanofibers, can be leveraged to dictate cell behavior. Most aspects of the scaffolds can be manipulated, from the orientation of the fibers in the scaffold to modifications of the nanofiber surface.Alignment of nanofibers was used to align cells and promote the differentiation and creation of myotubes from myoblasts. The diameter of nanofibers comprising a culture scaffold were shown to affect the morphology of astrocytes, and may have protective effects against reactive astrogliosis. Electrospun microfibers were surface modified to present binding proteins to cells, and were used as a non-biological neuron mimic to study CNS myelination. The data presented here are promising and provide many opportunities for future researchers to continue to understand how cells interact with the world around them.

Appendix 1 - Collagen Nanofibre anisotropy induces myotube differentiation and acetylcholine receptor clustering

Received: 8 July 2017 | Revised: 28 November 2017 | Accepted: 12 December 2017

DOI: 10.1002/term.2632

RESEARCH ARTICLE

WILEY

Collagen nanofibre anisotropy induces myotube differentiation and acetylcholine receptor clustering

Frank H. Kung[1] | David Sillitti[2] | Anil B. Shrirao[2] | David I. Shreiber[2,3] | Bonnie L. Firestein[1,3]

[1]Department of Cell Biology and Neuroscience, Rutgers University, Piscataway, NJ, USA

[2]Department of Biomedical Engineering, Rutgers University, Piscataway, NJ, USA

[3]Graduate Faculty in Biomedical Engineering, Rutgers University, Piscataway, NJ, USA

Correspondence
Bonnie L. Firestein, Department of Cell Biology and Neuroscience, Rutgers University, 604 Allison Road, Piscataway, NJ 08854, USA.
Email: firestein@biology.rutgers.edu

Funding information
New Jersey Commission on Spinal Cord Research, Grant/Award Number: CSCR14IRG005

Abstract

To create musculoskeletal tissue scaffolds for functional integration into host tissue, myotubes must be properly aligned with native tissue and spur the formation of neuromuscular junctions. However, our understanding of myoblast differentiation in response to structural alignment is incomplete. To examine how substrate anisotropy mediates myotube differentiation, we studied C2C12 myoblasts grown on aligned collagen substrates in the presence or absence of agrin. Myoblasts grown on microfluidically patterned collagen substrates demonstrated increased multinucleated myotubes and nicotinic acetylcholine receptor (AChR) clusters. However, agrin treatment did not synergistically increase differentiation of myoblasts seeded on these patterned collagen substrates. Myoblasts grown on aligned electrospun collagen nanofibres also demonstrated increased formation of multinucleated myotubes and AChR clusters, and agrin treatment did not increase differentiation of these cells. Using fluorescently labelled collagen nanofibres, we found that AChR clustered in cells grown on nanofibres with significantly higher anisotropy and that this clustering was eliminated with agrin treatment. Interestingly, anisotropy of substrate had no effect on the localization of AChRs along the myotube, suggesting that additional signalling pathways determine the specific location of AChRs along individual myotubes. Taken together, our results suggest a novel role for fibre anisotropy in myotube differentiation, specifically AChR clustering, and that anisotropy may guide differentiation by activating similar pathways to agrin. Our data suggest that agrin treatment is not necessary for differentiation and maturation of myoblasts into myotubes when myoblasts are grown on aligned collagen substrates.

KEYWORDS

muscle differentiation, musculoskeletal tissue engineering, myotube, neuromuscular junction, tissue engineering, topographical cues

1 | INTRODUCTION

There is an increased need for scaffolds for musculoskeletal tissue engineering because these tissues are routinely damaged in sports activities and during almost any surgical procedure (Järvinen & Lehto, 2012). To successfully integrate with host musculoskeletal tissue, scaffolds must meet a variety of requirements. For example, these tissue scaffolds must (a) allow myoblasts to properly differentiate into functional myotubes, (b) properly align with native tissue to repair or replace missing tissue from the patient, and (c) spur the formation of neuromuscular junctions (NMJs) for proper integration with host tissue peripheral nervous tissue. To create successful musculoskeletal tissue scaffolds, a better understanding of how materials and material properties affect myotube differentiation and NMJ formation is needed.

The use of topographical cues, that is, specifically creating aligned scaffolds, has been found to be beneficial for musculoskeletal tissue engineering. Seeding myoblasts on polydimethylsiloxane (PDMS) micropatterns or poly(lactic acid) scaffolds increases the differentiation of myoblasts into myotubes as demonstrated by increased myotube length, myotube striation, and decreased myoblast proliferation (Huang et al., 2006). Recently, a wide variety of electrospun aligned materials, including poly(epsilon-caprolactone)/collagen, poly(lactide-co-glycolide), poly(hydroxybutyrate), and chitosan, have been fabricated for musculoskeletal tissue engineering and have been used to

show that increased differentiation of myoblasts into myotubes occurs on multiple types of substrates (Aviss, Gough, & Downes, 2010; Choi, Lee, Christ, Atala, & Yoo, 2008; Ricotti et al., 2012). Furthermore, the topography of the substrate upon which myotubes are grown affects myoblast differentiation. For example, when myoblasts are grown on micropatterned PDMS substrates containing posts and trenches of various sizes and shapes, these topologies influence differentiation of the myoblasts into myotubes, and this cellular behaviour is explained by a simple geometrical model of myotube orientation (Gingras et al., 2009). Similarly, our group reported that the growth and differentiation of myoblasts in trenches 50 μm wide lead to individual myotube formation and differentiation, whereas growth of myoblasts in smaller or larger trenches causes formation of branching myotubes (Langhammer, Kutzing, Luo, Zahn, & Firestein, 2013; Langhammer, Zahn, & Firestein, 2010).

Despite the promise of alignment for increasing the integration of musculoskeletal tissue constructs with host tissue, research is lacking on identification of the specific molecular signalling pathways activated by topographical cues. Only in the past 3 years has it been demonstrated that alignment of myoblasts causes an upregulation of differentiation factors, such as MyoD, MyoG, and MyHC, and increased expression of important cell adhesion molecules, such as integrin α7β1, in vitro (Jana, Leung, Chang, & Zhang, 2014; McClure et al., 2016). In addition, it was recently demonstrated that myoblasts grown on aligned scaffolds show increased expression of dystrophin in vivo, thus potentially acting as a viable palliative for Duchenne's muscular dystrophy (Yang et al., 2014). These reports demonstrate that the local topography of the substrate on which myoblasts are seeded plays an important role in promoting the differentiation of myoblasts into myotubes, maturation of myotubes, and regulating integration with host tissues.

Although alignment increases the fusion of myoblasts into multinucleated myotubes, the effect of topographical cues upon the formation of nicotinic acetylcholine receptor (AChR) clusters and the formation of functional NMJs is unknown. Moreover, a subset of myotube differentiation factors that is upregulated after alignment plays important roles in the formation of AChR clusters, suggesting that alignment may spur the formation of AChR clusters or functional NMJs. For example, the transcription factor MyoD and adhesion protein integrin α7β1 are upregulated after alignment (McClure et al., 2016) and promote AChR clustering (Burkin, Kim, Gu, & Kaufman, 2000; Dutton, Simon, & Burden, 1993). However, more detailed analyses on how aligned topographical features affect AChR formation have not yet been performed. Understanding how NMJs form in response to aligned topographical features will inform us on how to create scaffolds that better integrate with host tissue.

Here, we investigate how alignment affects AChR clustering in myotubes formed from myoblasts seeded and grown on patterned collagen substrates and on a collagen nanofibre scaffold. Our results are the first to demonstrate that AChR clustering increases in response to substrate alignment, and we show that this increase in clustering likely signals via the same molecular pathway as does agrin to induce AChR clustering. Furthermore, we report that AChR clustering is sensitive to small differences in collagen nanofibre anisotropy. Finally, we find that this anisotropic sensitivity is limited to individual myotubes but does not induce region-specific expression of AChR clustering in myotubes.

2 | METHODS

2.1 | Microfluidic channel fabrication and collagen patterning

Microfluidic devices were fabricated as previously described (Shrirao, Kung, Yip, Cho, & Townes-Anderson, 2014). Briefly, silicon wafers were cleaned with 100% acetone, isopropyl alcohol, and ethanol for 10 min before dehydrating them in an oven (150 °C) overnight. SU-8 2025 (Microchem) was spin-coated onto the silicon wafers at a thickness of 41 μm. SU-8 was baked at 65 °C for 2 min and at 95 °C for 7 min before exposure to 160 mJ/cm^2 ultraviolet (UV) with a mask aligner EVG 620. Post-exposure, silicon wafers were baked at 65 °C for 1 min and at 95 °C for 3 min. Wafers were developed in SU-8 developer for 5 min, washed with 100% isopropyl alcohol, and hard baked overnight in an oven at 150 °C. Silicon masters were then silanized for 1 hr with (tridecafluoro-1,1,2,2-tetrahydrooctyl)-1-trichlorosilane vapours (United Chemical Technology Inc., Levittown, PA, USA) under vacuum. PDMS (Sylgard 184, Dow Corning Inc., USA) elastomer and curing agent were mixed in a 10:1 weight ratio, poured over the top of the silicon masters, degassed for 30 min, and then polymerized in a 65 °C oven for at least 2 hr before being cut out from the silicon wafers. One-millimetre inlets and outlets were punched into each PDMS device and then sterilized with 70% ethyl alcohol, washed 3 times with water, and placed under UV radiation for 30 min prior to use.

Collagen was patterned using the microfluidic devices as previously reported (Shrirao et al., 2014; Shrirao et al., 2017). Briefly, sterilized PDMS microfluidic devices were placed onto cleaned 22-mm square glass coverslips in a 6-well cell culture plate. Collagen type 1 solution (30 μl of 0.01%; Sigma Aldrich, cat#: C8919) was diluted in phosphate-buffered saline (PBS) and placed onto the inlet and outlet of the microfluidic device, and then the device was placed into a vacuum chamber for 10 min. The vacuum was removed, and the entire apparatus was placed into a cell culture incubator overnight. Excess collagen was aspirated from the microfluidic devices, and the device was removed from the glass coverslip and discarded. Glass coverslips were washed 3 times with PBS. Confirmation of collagen patterning was performed by staining with 50 μM N-Hydroxysuccinimide (NHS)-fluorescein (5/6-carboxyfluorescein succinimidyl ester) mixed isomer (Thermo-Fisher, cat#: 46409) for 1 hr and then subsequently washing 3 times with PBS, mounting the 22-mm square coverslips with Fluoromount G (Southern Biotech, cat# 0100-01), and imaging on an EVOS® FL microscope (Thermo-Fisher, Cat#: AMF4300) at 40× magnification. Patterned and unpatterned coverslips to be used for cell culture were coated overnight with a 1% bovine serum albumin solution in PBS. Patterned glass coverslips were washed 3 times with PBS and used for subsequent experiments.

2.2 | Production and characterization of electrospun collagen nanofibres

Solutions of 8 wt% lyophilized collagen (Bovine type I, Kensey Nash, Exton, PA, USA) were prepared in 1,1,1,3,3,3-hexafluoro-2-propanol (Oakwood Chemical, Estill, SC, USA) (Boland et al., 2004) for 24 hr. Electrospinning was performed onto either a grounded metal plate or a grounded rotating metal drum, 17 cm from the needle tip, at speeds of 865 m/min at the drum surface. Electrospinning solution was ejected at 0.25 ml/hr with an accelerating voltage of 15 kV. Scanning electron microscopy images (i.e., as shown in Figure 1) were prepared and analysed using a Zeiss Sigma field emission scanning electron microscope.

2.3 | Fluorescent labelling of collagen nanofibres

Collagen nanofibres were fluorescently labelled using Alexa Fluor™ 555 NHS ester (succinimidyl ester; Thermo Fisher, cat# A37571). Collagen nanofibres were sterilized with UV irradiation for 30 min. Collagen nanofibres were then labelled with 50 μM Alexa Fluor™ 555 NHS ester (succinimidyl ester) dissolved in 0.5% dimethyl sulfoxide and PBS. Plates were protected from ambient light and placed onto a shaker for 1 hr. Collagen nanofibres were then washed 3 times with PBS before seeding with C2C12 myoblasts as described below.

2.4 | Cell growth and maintenance

C2C12 mouse myoblast cells (American Type Culture Collection, Manassas, VA, USA) were grown in T75 flasks in growth medium (Dulbecco's modified Eagle's medium + 10% fetal bovine serum). Only cultures below Passage 15 were used. At ~70% confluency, myoblasts were trypsinized and diluted to 500,000 cells per patterned coverslip or 200,000 cells per well for coverslips with or without nanofibre mats or random and aligned collagen nanofibres. At day in vitro (DIV) 2, growth medium was aspirated from each well and replaced with differentiation medium (Dulbecco's modified Eagle's medium + 2% horse serum). At DIV7, cells on mats were fixed with 4% paraformaldehyde in PBS and immunostained with rabbit anti-desmin (1:500; Sigma Aldrich, cat# D1033), α-bungarotoxin Alexa Fluor® 488 conjugate (Thermo-Fisher, cat# B13422), and Hoechst 33225. Myotubes were imaged at 200× with an EVOS® FL microscope (Thermo-Fisher, cat# AMF4300). Myotube formation was evaluated by manual counting of a number of multinucleated cells, cell nuclei, number of AChR clusters, and AChR cluster size.

2.5 | Analysis of nanofibre anisotropy

Nanofibre isotropy was analysed using a modified version of the FibrilJ plugin developed by Sokolov, Belousov, Bondarev, Zhouravleva, and Kasyanenko (2017). Briefly, fluorescently labelled nanofibres were imaged at 200× with an EVOS® FL microscope. Labelled images were divided into 50 pixel × 50 pixel segments, and each segment was evaluated for anisotropy using the FibrilJ plugin (i.e., as shown in Figure 4). To correlate myotube growth and differentiation with nanofibre anisotropy, regions of nanofibres with differentiated myotubes were segmented into 50 pixel × 50 pixel segments and evaluated by FibrilJ for anisotropy and fibre orientation (i.e., as shown in Figure 4).

2.6 | Statistical analysis

One-way analysis of variance followed by the appropriate multiple comparisons test was performed using GraphPad Prism 7.0 (GraphPad, La Jolla, CA, USA). A p value <.05 was considered significant.

3 | RESULTS

3.1 | PDMS patterning and collagen nanofibre fabrication

To examine how myoblast geometry affects myotube differentiation and clustering of nicotinic AChRs, PDMS microfluidic patterning of collagen substrates or aligned collagen nanofibre scaffolds was used. Patterned collagen substrates were fabricated as previously described utilizing vacuum-assisted patterning (Shrirao et al., 2014; Shrirao et al., 2017). Microfluidic devices used for this experiment contained channels of 10 μm width, which are separated by walls of 200 μm thickness, creating patterned collagen. Collagen patterning on glass coverslips was confirmed via staining with NHS-fluorescein (5/6-carboxyfluorescein succinimidyl ester; Figure 1a–c). Each microfluidic channel created similar patterns of single lanes of collagen substrate ~10 μm in width. For nanofibres, collagen was electrospun in both random and aligned formats (Figure 1d,e). Collagen nanofibres were fabricated from a solution of collagen in hexafluoroisopropanol by electrospinning the fibres onto aluminium foil attached to either a flat grounding plate (random fibres) or a high-speed rotating mandrel as the grounding mechanism (aligned fibres; Aviss et al., 2010; Choi et al., 2008). Alignment of collagen nanofibres was confirmed via scanning electron microscopy (Figure 1b).

3.2 | Effects of patterned collagen and agrin on differentiation of myotubes and clustering of AChRs are not additive

To determine the effect of collagen substrate alignment on myotube differentiation and AChR cluster formation, unpatterned and patterned collagen substrates (fabricated by microfluidic patterning methods as previously described; Shrirao et al., 2014; Shrirao et al., 2017) were seeded with C2C12 myoblasts, and the myoblasts were differentiated into myotubes via serum deprivation after DIV2. After fixation, the cells were stained for nuclei and AChR clusters with Hoechst 3352 and α-bungarotoxin conjugated to Alexa Fluor 488, respectively. Multinucleated myotubes could be clearly distinguished from surrounding undifferentiated cells (Figure 2a). To control for initial cell number in each condition, individual nuclei were counted in each image and normalized to unpatterned collagen in each experiment. No statistically significant differences in the number of nuclei were observed, indicating that cell adhesion and growth do not differ between conditions. The addition of agrin to cell differentiation medium did not affect the number of nuclei (Figure 2b).

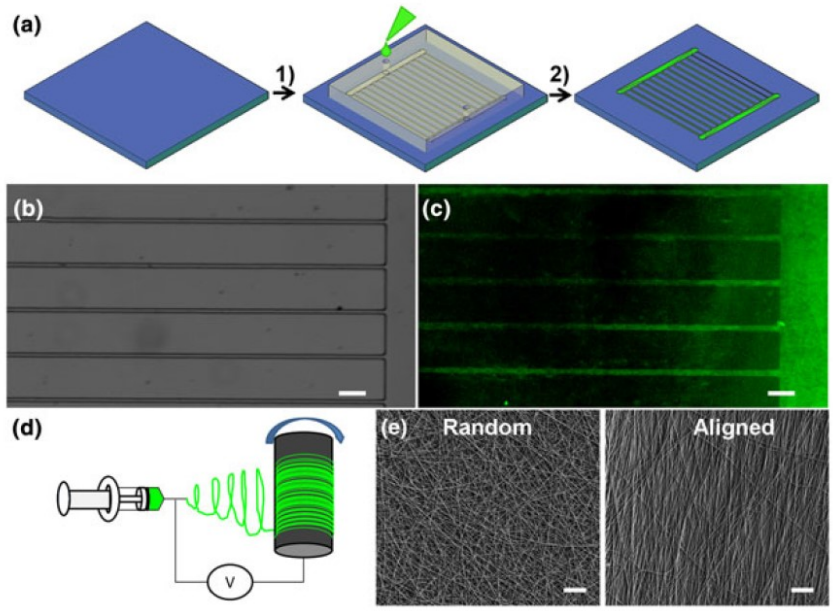

FIGURE 1 Polydimethylsiloxane (PDMS) patterning and electrospinning set-up. (a) Glass coverslips were patterned using vacuum-assisted PDMS microfluidic devices as follows: (1) Microfluidic devices were placed onto clean 22-mm glass coverslips, and 20 µl of droplet of 0.01% collagen solution was injected into the microfluidic channels using the vacuum-assisted protein patterning technique. (2) After incubation at 37 °C for 24 hr, PDMS microfluidic devices were removed from the coverslip and coated with 2% bovine serum albumin in phosphate-buffered saline solution for another 24 hr prior to seeding with C2C12 myoblasts. (b) Microfluidic device. Microfluidic device contained channels 10 µm in width separated by 200 µm. Scale bar = 100 µm. (c) Collagen patterned by microfluidic device. Collagen was stained with NHS-succinylmide-ester fluorescein. Collagen patterning was confirmed by fluorescent imaging. Scale bar = 100 µm. (d) Electrospinning set-up. Collagen solution was electrospun onto a high-speed rotating mandrel to align collagen fibres. A high-voltage power source was attached to a syringe pump and to the metal mandrel. The syringe was placed onto the pump, which slowly injected solution into the high-voltage environment, causing collagen nanofibres to adhere to the rotating metal mandrel to align the collagen nanofibres. (e) Scanning electron microscopy of electrospun collagen nanofibres. Random nanofibres were electrospun onto a grounded metal plate, whereas aligned nanofibres were spun onto a grounded rotating metal mandrel. Scale bars = 10 µm [Colour figure can be viewed at wileyonlinelibrary.com]

We then quantitated the number of individual multinucleated myotubes, as identified by staining with Hoechst 3352 and α-bungarotoxin conjugated to Alexa Fluor 488. AChR clusters were distinguishable from background staining, allowing for identification of individual myotubes (Figure 2a). Growth on aligned collagen increased the number of multinucleated myotubes when normalized to those grown on unpatterned collagen (Figure 2b), suggesting that alignment promotes differentiation. In contrast to what we expected (Barik, Zhang, Sohal, Xiong, & Mei, 2014; Bezakova & Ruegg, 2003; Martin & Sanes, 1997; Trinidad, Fischbach, & Cohen, 2000; Weston, Teressa, Weeks, & Prives, 2007), the addition of agrin to the medium did not increase the number of multinucleated myotubes on the aligned collagen samples, suggesting that agrin treatment may occlude the effect of patterned collagen on differentiation. In unpatterned collagen samples, agrin significantly increased the number of multinucleated myotubes, confirming its activity and consistent with previous work (Aviss et al., 2010; Choi et al., 2008; Gingras et al., 2009; Yang et al., 2014).

Because AChR clustering serves as a marker for myotube maturity and is crucial for the proper development of NMJs (Menon, Carrillo, & Zinn, 2013; Tintignac, Brenner, & Rüegg, 2015), we examined the formation of AChR clusters when cells were grown on unpatterned and aligned collagen in the absence or presence of agrin. We quantitated the total number of AChR clusters divided by total number of multinucleated myotubes in each image and normalized to this metric to that of cells grown on unpatterned collagen. Collagen alignment or agrin addition to the medium significantly increased the number of AChR clusters per myotube (Figure 2b). However, when cells were grown on aligned collagen and simultaneously treated with agrin, the effect of the individual treatments was not additive, suggesting a shared mechanism between the two treatments or a maximum threshold of AChR clustering (Figure 2b). Furthermore, the average area of each AChR cluster increased in response to agrin regardless of collagen patterning, although collagen alignment alone had no effect (Figure 2b). Taken together, these data suggest that the size of AChR clusters may be controlled by a molecular pathway activated specifically by agrin but not by alignment.

3.3 | Collagen nanofibres and agrin treatment promote myotube differentiation and AChR clustering

Because the micropatterned collagen substrate on the glass slides is not a biologically relevant system for tissue engineering, we constructed collagen nanofibres and seeded and differentiated myoblasts on these fibres. C2C12 myoblasts were seeded on random and aligned

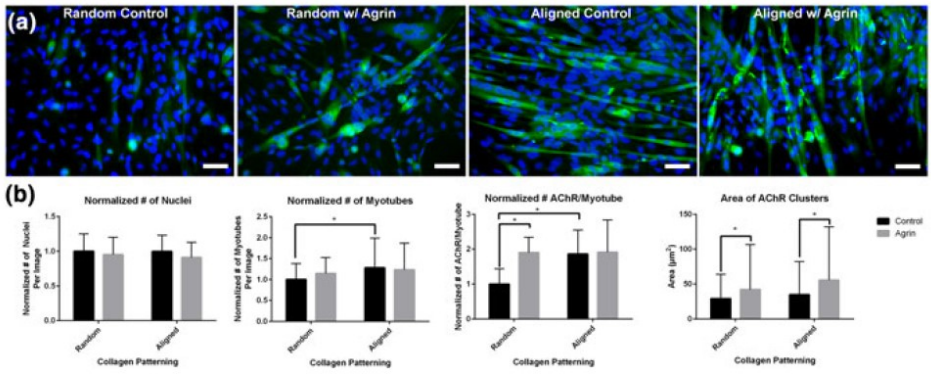

FIGURE 2 Differentiation of myotubes and clustering of acetylcholine receptors (AChRs) by collagen patterned by polydimethylsiloxane and agrin are not additive. (a) Example myotubes formed on random or aligned patterns of collagen on glass coverslips in the absence or presence of agrin. From left to right: C2C12 cells plated onto randomly aligned collagen patterns, C2C12 cells plated on aligned nanofibres, C2C12 cells plated onto randomly aligned collagen patterns and treated with agrin, and C2C12 cells plated on aligned collagen patterns and treated with agrin. Scale bars = 50 μm. Myotubes were stained for AChRs (green) and nuclei (blue) with α-bungarotoxin Alexa Fluor 488 and Hoechst 35288, respectively. (b) Differentiation of myotubes and clustering of AChRs in the four different conditions. Nuclei were counted in each image by staining with Hoechst 35288, thresholding in ImageJ, and utilizing the particle analysis plugin. Number of multinucleated myotubes was examined by analysing AChR staining with α-bungarotoxin Alexa Fluor 488 and determining the presence of multiple nuclei in each cell. AChR clusters were counted in each image and divided by the total number of myotubes per image. Quantification of differentiation was normalized to myotubes grown on randomly patterned collagen. No significant increase in the number of myotubes was seen in cultures grown on aligned collagen whether or not agrin was present. Error bars = standard deviation. $n = 4$ cultures, 60 images per culture. $^*p < .05$ determined by one-way analysis of variance and Tukey's post hoc analysis [Colour figure can be viewed at wileyonlinelibrary.com]

collagen nanofibres and differentiated by serum deprivation into myotubes (Figure 3a). Cultures were fixed and stained for nuclei and AChRs, and similar to the analysis of cells grown on patterned collagen substrates, multinucleated myotubes and AChR clusters were quantified and normalized to those present on random nanofibres (Figure 3a).

We observed that significantly fewer nuclei were present on aligned collagen nanofibres than were present on the random collagen nanofibres (Figure 3b). Interestingly, despite the fact that fewer nuclei were present, the number of multinucleated myotubes was greater when cells were grown on aligned collagen samples in the absence or

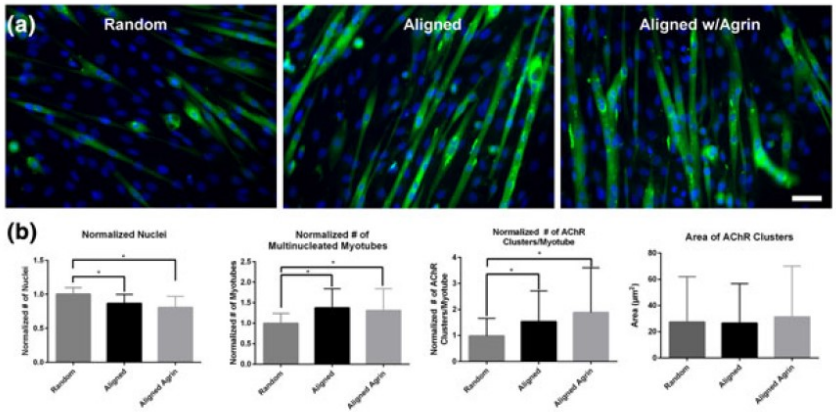

FIGURE 3 Differentiation of myotubes and acetylcholine receptor (AChR) clustering are enhanced by collagen nanofibre alignment and agrin in a nonadditive manner. (a) Example myotubes that form on collagen electrospun nanofibres. From left to right: Myotubes grown on randomly electrospun nanofibres, myotubes grown on aligned nanofibres, and myotubes grown on aligned nanofibres and treated with agrin. Myotubes are stained for AChR and nuclei with α-bungarotoxin Alexa Fluor 488 (green) and Hoechst 35288 (blue), respectively. Scale bar = 50 μm. (b) Quantitation of myotube differentiation and AChR formation in conditions shown in panel (a). Nuclei were counted in each image by staining with Hoechst 35288, thresholding in ImageJ, and utilizing the particle analysis plugin. Number of multinucleated myotubes was examined by analysing AChR staining with α-bungarotoxin Alexa Fluor 488 and examining the presence of multiple nuclei in each cell. AChR clusters were counted in each image and divided by the total number of myotubes per image. Quantification of differentiation was normalized to that of myotubes grown on randomly electrospun nanofibres in the absence of agrin. Error bars = standard deviation. $n = 4$ cultures, 60 images per culture. $^*p < .05$ determined by one-way analysis of variance and Tukey's post hoc analysis [Colour figure can be viewed at wileyonlinelibrary.com]

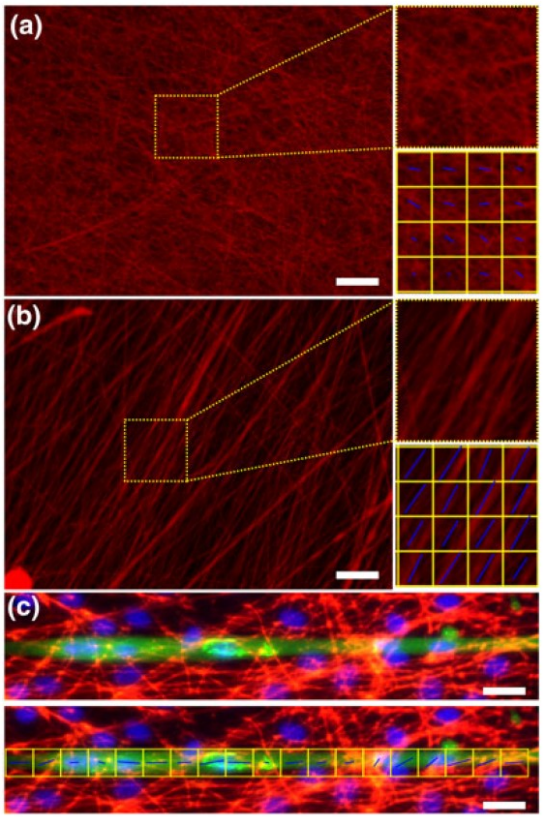

FIGURE 4 Example of measurement of collagen nanofibre alignment. Collagen nanofibres were fluorescently labelled with Alexa Fluor™ 555 NHS ester (succinimidyl ester), allowing for live monitoring using fluorescent microscopy. Alignment of collagen nanofibres was analysed via FibrilJ by image segmentation. The lengths of blue lines indicate the level of anisotropy measured from each yellow region of interest. Orientation of blue lines indicates average fibril orientation for the particular segment. (a) Anisotropy analysis of random electrospun collagen nanofibres. Scale bar = 50 μm. (b) Anisotropy analysis of aligned collagen nanofibres. Scale bar = 50 μm. (c) Anisotropy analysis of collagen nanofibres underlying individual myotubes stained for acetylcholine receptor and nuclei with α-bungarotoxin 488 and Hoechst 35288, respectively. Scale bars = 25 μm [Colour figure can be viewed at wileyonlinelibrary.com]

presence of agrin (Figure 3b), indicating an increase in differentiation from myoblasts to myotubes. Treatment with agrin alone promoted the same changes to nuclei and number of myotubes; however, treatment of cells grown on aligned nanofibres with agrin resulted in the same degree of differentiation of myoblasts to myotubes that resulted from either condition alone. These data further suggest a shared mechanism between alignment and agrin in promoting differentiation.

Because patterned collagen substrate increases AChR clustering in multinucleated myotubes, we asked whether aligned substrates promote AChR cluster formation. We quantitated AChR clusters by dividing total number of multinucleated myotubes per image and normalizing to this metric from cells grown on random collagen nanofibres and found that the number of AChR clusters per myotube increased in cultures grown on aligned collagen myotubes whether or not the cultures were treated with agrin (Figure 3b), suggesting a shared mechanism between the two treatments or a maximum threshold of AChR clustering. In contrast to what we observed when cultures were grown on patterned collagen, the size of AChR clusters did not significantly differ in any experimental condition, suggesting that collagen nanofibre alignment and agrin treatment do not enhance AChR cluster size under these experimental conditions (Figure 3b).

3.4 | Collagen nanofibre anisotropy changes after cultured with C2C12 cells for 2 days

Because it is possible that growth and differentiation of myoblasts can remodel the collagen nanofibres on which they are grown, we examined the structure of electrospun collagen nanofibres during differentiation of myoblasts or in response to factors secreted by the cells. Collagen nanofibres were fluorescently labelled with either NHS-fluorescein (5/6-carboxyfluorescein succinimidyl ester) or Alexa Fluor™ 555 NHS ester (succinimidyl ester), allowing for live monitoring of collagen nanofibre structure using fluorescent microscopy (Figure 4). Growth and differentiation of myoblasts had no effect on the anisotropy of random fibres; however, myoblast growth decreased the anisotropy of aligned fibres over the 2-day post-seeding, and this decrease was observed regardless of whether agrin was present (Figure 5a,b). These data suggest that myoblast growth and differentiation may act to remodel the surrounding substrate.

3.5 | Myotube differentiation correlates with fibre anisotropy

Because C2C12 cells alter collagen nanofibre anisotropy (Figure 5a,b), we determined how collagen nanofibre anisotropy affects the expression of and the localization of AChR clusters by dividing each myotube into even regions and measuring collagen nanofibre anisotropy of those regions using a modified version of FibrilJ ImageJ plugin. In addition, we quantified total nanofibre density by measuring the fluorescent intensity of each region fluorescing Alexa Fluor™ 555 NHS ester. For all quantifications, measurements were normalized to those of myotubes on random collagen nanofibres. In myotubes seeded on randomly electrospun collagen nanofibres, myotubes with AChR clusters occurred less frequently on nanofibres with higher anisotropy (Figure 6a,b). However, in myotubes seeded on aligned electrospun collagen nanofibres, myotubes with AChR clusters formed on nanofibres with high levels of anisotropy more frequently than did those without AChR clusters (Figure 6b). This difference in myotube preference for fibre anisotropy did not occur in myotubes on aligned nanofibres that were treated with agrin. Furthermore, myotubes containing AChR clusters only grow on higher nanofibre density when grown on random nanofibres. These data suggest that myotube fusion results from different mechanisms when myoblasts are seeded on random collagen nanofibres versus aligned nanofibres.

As cellular events are often regulated by the local environment, we examined if local collagen nanofibre anisotropy correlates with the

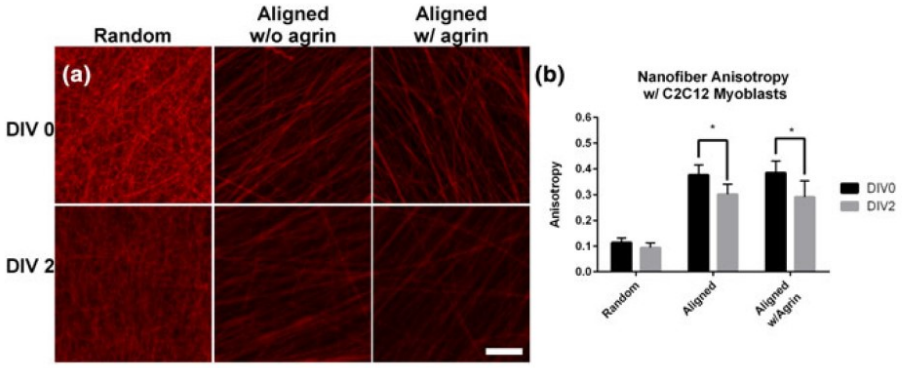

FIGURE 5 Collagen nanofibre anisotropy decreases after cultured with C2C12 cells for 2 days. (a) Example nanofibres fluorescently labelled with NHS-ester Alexa Fluor 555. Top row: Two sets of fibres on day in vitro (DIV) 0. Bottom row: Two sets of fibres on DIV2. Left: Randomly aligned nanofibres seeded with C2C12 myoblasts. Centre: Aligned nanofibres seeded with C2C12 myoblasts. Right: Aligned nanofibres seeded with C2C12 myoblasts and treated with agrin. Scale bars = 50 μm. (b) Anisotropy measurements of fibres seeded with C2C12 myoblasts in panel (a). Error bars = standard deviation. n = 4 cultures, 5 images per time point per culture. *p < .05 as determined by one-way analysis of variance and Tukey's post hoc analysis [Colour figure can be viewed at wileyonlinelibrary.com]

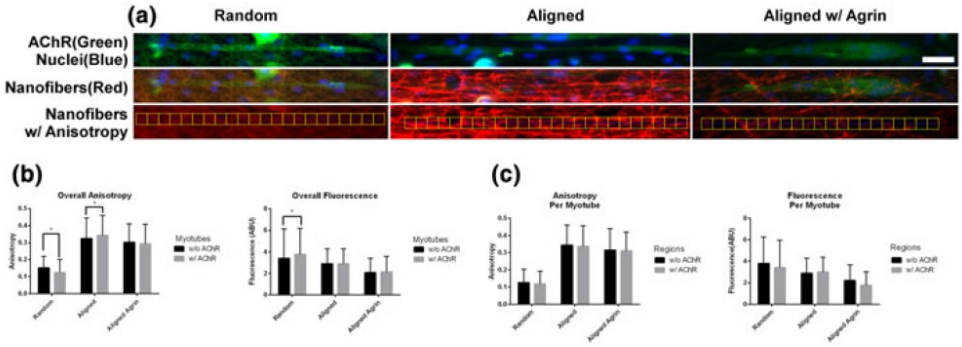

FIGURE 6 Myotube differentiation correlates with fibre anisotropy. (a) Example myotubes grown on fluorescently labelled collagen nanofibres. Acetylcholine receptor (AChR) clusters identified via staining with α-bungarotoxin 488 after growth and differentiation on labelled collagen nanofibres. Nanofibres were then imaged, and their structure was evaluated using FibriIJ anisotropy analysis. Scale bar = 50 μm. (b) On average, myotubes containing AChR clusters prefer to grow on collagen nanofibres with higher levels of anisotropy than do myotubes without AChR clusters. This effect is attenuated with agrin treatment. Individual myotubes with higher levels of AChR clusters have no preference for growth on fibres with higher anisotropy. No significant difference in overall collagen nanofibre fluorescence was found in myotubes either without AChR clusters or with AChR clusters on aligned nanofibres or aligned nanofibres with agrin containing differentiation medium. No significant difference in overall collagen nanofibre fluorescence was found on aligned nanofibres or aligned nanofibres with agrin containing differentiation medium. Error bars = standard deviation. n = 4 cultures, 60 images per culture. *p < .05 determined by one-way analysis of variance and Tukey's post hoc analysis. ABU = arbitrary units. (c) Specific regions of myotubes with and without AChR clusters do not show a preference for aligned nanofibres. No significant difference was found between fluorescence per myotube for cells on aligned nanofibres versus cells on aligned nanofibres plus agrin treatment. Error bars = standard deviation. *p < .05 determined by one-way analysis of variance and Tukey's post hoc analysis. n = 4 cultures, 60 images per culture. ABU = arbitrary units [Colour figure can be viewed at wileyonlinelibrary.com]

localization of AChR cluster formation. Collagen nanofibre anisotropy was compared in regions of myotubes with AChR clusters or without AChR clusters (Figure 6a). In these regions, no correlation was found for cells grown on random electrospun nanofibres, aligned nanofibres, or aligned nanofibres in the presence of agrin. These data suggest that although the structure of collagen nanofibres may preferentially increase the expression of AChR clusters in individual myotubes, these differences in structural anisotropy in collagen nanofibres do not promote local clustering of AChR in myotubes. Additionally, the addition of agrin did not promote local effects of nanofibre anisotropy (Figure 6b). As a control, we determined the amount of nanofibres on which myotubes with and without AChR clusters grew and determined that in each condition, both classes of myotubes covered similar density of nanofibres as determined by fluorescence of fibres (Figure 6c). Taken together, this analysis suggests that in this setting, the amount of collagen nanofibre on which myotubes are grown plays a less important role in AChR cluster formation than collagen nanofibre structural anisotropy.

4 | DISCUSSION

4.1 | Topographical alignment and agrin share similar myotube differentiation pathways

In our study, we demonstrated that topographical cues increase both myotube differentiation and the formation of AChR clusters. We found that this increase in myotube differentiation occurs when myoblasts are plated on either aligned collagen substrates on glass coverslips or electrospun aligned collagen nanofibres. Specifically, our data are the first to examine how cell substrate topography affects the formation of AChR clusters and supplies evidence that alignment- and agrin-promoted AChR clustering shares a common signalling mechanism. Our work suggests that this specific topographically sensitive signalling pathway may interact with other pathways utilized by myotubes to form AChR clusters and subsequently NMJs. In specific, we demonstrate the lack of additional myotube differentiation and AChR formation when alignment and agrin are applied together to differentiating myotubes. We believe that this is the first report demonstrating that AChR clustering increases in response to substrate alignment.

Previous work demonstrated that alignment leads to the upregulation of the integrin receptor α7β1 and that this receptor is a crucial component of the differentiation pathway during myotube alignment (McClure et al., 2016; Zhang, Sun, Lee, Abdeen, & Kilian, 2016). Additionally, integrin receptor α7β1 specifically activates the myotube transcription factor MyoD (McClure et al., 2016; Zhang et al., 2016), which is vital for proper formation of both multinucleated myotubes and AChR cluster formation (Piette, Bessereau, Huchet, & Changeux, 1990; Rudnicki & Jaenisch, 1995; Weintraub, 1993). From our study, we propose a model of myotube differentiation and interaction between alignment and agrin that demonstrates how alignment and agrin can interact along the same pathways and thus not increase AChR formation in aligned samples (Figure 7).

In this model, aligned substrates increase the expression of integrin α1β7 (McClure et al., 2016), and downstream signalling is key to inducing agrin-related AChR clustering (Bezakova & Ruegg, 2003; Burkin et al., 2000; Martin & Sanes, 1997). Alignment increases integrin signalling and may subsequently begin a cascade of signalling, leading to an eventual downregulation of the late differentiation factor paired box protein (PAX7) and upregulation of late differentiation factor MyoD (McClure et al., 2016). The addition of agrin to myoblast cell cultures leads to additional AChR formation via the MyoD pathway (Anderson & Grow, 2012) but not in myoblast cultures where MyoD is already activated by topographical alignment.

Our work suggests that other molecules may be necessary to increase AChR cluster formation in myoblasts grown on aligned substrates. We speculate that these molecules include laminin (Burkin et al., 2000; Weston et al., 2007), WNT3 (Barik et al., 2014; Henriquez et al., 2008; Korkut & Budnik, 2009), and neuregulin (Buonanno & Fischbach, 2001; Trinidad et al., 2000), which co-stimulate AChR formation over AChR formation by agrin alone. Therefore, it may be necessary to use co-stimulators, such as the ones listed above or others, to induce further AChR cluster formation in developing myoblasts and to create functional NMJ for musculoskeletal tissue-engineered constructs.

In addition, future studies will determine the level of anisotropy necessary to activate these signalling pathways and determine if different levels of anisotropy affect the response to these co-stimulatory molecules. Other than comparing patterned and unpatterned conditions, our study did not determine the levels of anisotropy needed to affect AChR clustering or how anisotrophy affects the response to co-stimulatory molecules.

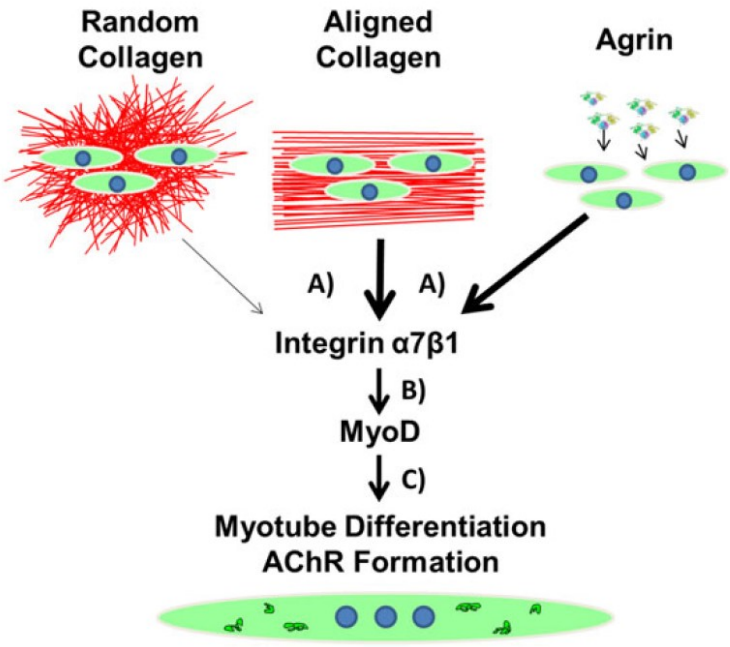

FIGURE 7 Proposed model for myotube differentiation and acetylcholine receptor (AChR) clustering promoted by collagen alignment and agrin. (A) Aligned collagen nanofibres and agrin both activate integrin α7β1 receptors (Burkin et al., 2000; Martin & Sanes, 1997; McClure et al., 2016; Zhang et al., 2016), (B) which in turn activate MyoD (McClure et al., 2016; Zhang et al., 2016). (C) MyoD subsequently increases myoblast differentiation and myotube formation (Anderson & Grow, 2012; Piette et al., 1990; Rudnicki & Jaenisch, 1995; Weintraub, 1993). MyoD then acts to increase AChR clustering in differentiated myotubes (Anderson & Grow, 2012; Piette et al., 1990; Rudnicki & Jaenisch, 1995; Weintraub, 1993) [Colour figure can be viewed at wileyonlinelibrary.com]

4.2 | Topographical cues affect levels of AChR clustering but not localization in individual myotubes

Our study demonstrates that individual myotubes are sensitive to collagen nanofibre structure and that increases in nanofibre anisotropy upregulate the expression of AChR clusters within individual myotubes. Furthermore, this sensitivity to anisotropy is abrogated when agrin is applied to the collagen myotubes, further providing evidence that the signalling pathways that induce AChR clustering by alignment are shared with those activated by agrin.

Despite the finding that AChR clustering in individual myotubes is sensitive to collagen nanofibre anisotropy, we did not find evidence of collagen nanofibre structure anisotropy affecting AChR cluster localization along the myotube. This suggests that although alignment may increase expression of integrin receptors and other myotube differentiating factors, the proteins that are important in determining the final localization of AChRs along a myotube are not sensitive to alignment. These factors may include extracellular receptors or cell adhesion molecules, such as Low-density lipoprotein receptor-related protein 4 (LRP4) (Barik et al., 2014) and neural cell adhesion molecules (NCAMs) (Covault & Sanes, 1986), or cytoskeletal associated proteins, such as muscle-specific kinase (MuSK) (Hubbard & Gnanasambandan, 2013; Trinidad et al., 2000), dystroglycan, and isoforms of protein kinase C (PKC) (Lanuza et al., 2014), all of which are important in the final formation and stabilization of NMJ at specific sites in the myotube.

The ability to control region-specific expression of AChR clusters in scaffolds may be important to specifically guide regenerating peripheral neurons to regions of the myotube where AChRs are developing and clustering. Doing so may increase the number of functional NMJs in the tissue-engineered construct and increase functionality. From our study, it appears that altering the topography of a scaffold is not sufficient to enhance AChR formation to a specific region of myotube or scaffold. Our results suggest that alternative strategies, such as spatially specific stimulation with AChR clustering molecules, are necessary for designing constructs with topographically localized AChR clusters. For example, microfluidics have been used to specifically control the regions of myotubes exposed to extracellular agrin and, hence, induce AChR cluster formation in areas with greater local concentrations of agrin (Tourovskaia, Kosar, & Folch, 2006; Tourovskaia, Li, & Folch, 2008). Thus, scaffolds may require specific regions primed with stimulatory molecules (Whitehead & Sundararaghavan, 2014) to enhance expression of AChR clusters in specific regions.

4.3 | AChR cluster size in patterned collagen and in collagen nanofibres

AChR cluster size is significantly increased in the presence of agrin when myoblasts are differentiated into myotubes on either random or aligned collagen on glass coverslip; however, cluster size does not significantly increase in the presence of agrin in myoblasts grown on collagen nanofibre scaffolds. It is possible that collagen substrates coated on glass slides may not activate signalling pathways that regulate cluster size that are activated in myoblasts grown on collagen nanofibre scaffolds. It was previously shown that agrin-induced signalling plays a role in initial and long-term clustering of AChRs and that cluster size is dependent upon this long-term signalling (Bezakova & Ruegg, 2003). In addition to agrin, other factors, such as Src, Fyn, Yes, rapsyn, and calpain, play important roles in stabilization of AChR clusters (Chen et al., 2007; Smith, Mittaud, Prescott, Fuhrer, & Burden, 2001), and whether or not these factors are activated in the presence of collagen nanofibres is currently unknown. Identification of the effector pathways stimulated by collagen nanofibres is the subject of future study.

ACKNOWLEDGEMENTS

This work was funded by New Jersey Commission on Spinal Cord Research Grant CSCR14IRG005 (to B. L. F.). We would like to thank Dr. Jeffrey D. Zahn (Rutgers University) for the gracious use of the BioMEMS facility.

CONFLICT OF INTEREST

The authors have declared that there is no conflict of interest.

ORCID

Bonnie L. Firestein http://orcid.org/0000-0002-1679-3565

REFERENCES

Anderson, E. E., & Grow, W. A. (2012). MyoD and Myogenin are required for agrin-induced AChR clustering. *The FASEB Journal*, *26*(1 Supplement), 919.912.

Aviss, K., Gough, J., & Downes, S. (2010). Aligned electrospun polymer fibres for skeletal muscle regeneration. *European Cells & Materials*, *19*, 193–204.

Barik, A., Zhang, B., Sohal, G. S., Xiong, W. C., & Mei, L. (2014). Crosstalk between agrin and Wnt signaling pathways in development of vertebrate neuromuscular junction. *Developmental Neurobiology*, *74*(8), 828–838.

Bezakova, G., & Ruegg, M. A. (2003). New insights into the roles of agrin. *Nature Reviews Molecular Cell Biology*, *4*(4), 295–309.

Boland, E. D., Matthews, J. A., Pawlowski, K. J., Simpson, D. G., Wnek, G. E., & Bowlin, G. L. (2004). Electrospinning collagen and elastin: Preliminary vascular tissue engineering. *Frontiers in Bioscience*, *9*(1422), e32.

Buonanno, A., & Fischbach, G. D. (2001). Neuregulin and ErbB receptor signaling pathways in the nervous system. *Current Opinion in Neurobiology*, *11*(3), 287–296.

Burkin, D. J., Kim, J. E., Gu, M., & Kaufman, S. J. (2000). Laminin and alpha7beta1 integrin regulate agrin-induced clustering of acetylcholine receptors. *Journal of Cell Science*, *113*(16), 2877–2886.

Chen, F., Qian, L., Yang, Z.-H., Huang, Y., Ngo, S. T., Ruan, N.-J., … Ding, Y.-Q. (2007). Rapsyn interaction with calpain stabilizes AChR clusters at the neuromuscular junction. *Neuron*, *55*(2), 247–260.

Choi, J. S., Lee, S. J., Christ, G. J., Atala, A., & Yoo, J. J. (2008). The influence of electrospun aligned poly(epsilon-caprolactone)/collagen nanofiber meshes on the formation of self-aligned skeletal muscle myotubes. *Biomaterials*, *29*(19), 2899–2906.

Covault, J., & Sanes, J. R. (1986). Distribution of N-CAM in synaptic and extrasynaptic portions of developing and adult skeletal muscle. *The Journal of Cell Biology*, *102*(3), 716–730.

Dutton, E. K., Simon, A. M., & Burden, S. J. (1993). Electrical activity-dependent regulation of the acetylcholine receptor delta-subunit gene, MyoD, and myogenin in primary myotubes. *Proceedings of the National Academy of Sciences*, *90*(5), 2040–2044.

Gingras, J., Rioux, R. M., Cuvelier, D., Geisse, N. A., Lichtman, J. W., Whitesides, G. M., … Sanes, J. R. (2009). Controlling the orientation and synaptic differentiation of myotubes with micropatterned

substrates. *Biophysical Journal*, *97*(10), 2771–2779. https://doi.org/10.1016/j.bpj.2009.08.038.

Henriquez, J. P., Webb, A., Bence, M., Bildsoe, H., Sahores, M., Hughes, S. M., & Salinas, P. C. (2008). Wnt signaling promotes AChR aggregation at the neuromuscular synapse in collaboration with agrin. *Proceedings of the National Academy of Sciences of the United States of America*, *105*(48), 18812–18817. https://doi.org/10.1073/pnas.0806300105.

Huang, N. F., Patel, S., Thakar, R. G., Wu, J., Hsiao, B. S., Chu, B., … Li, S. (2006). Myotube assembly on nanofibrous and micropatterned polymers. *Nano Letters*, *6*(3), 537–542.

Hubbard, S. R., & Gnanasambandan, K. (2013). Structure and activation of MuSK, a receptor tyrosine kinase central to neuromuscular junction formation. *Biochimica et Biophysica Acta (BBA) - Proteins and Proteomics*, *1834*(10), 2166–2169. https://doi.org/10.1016/j.bbapap.2013.02.034.

Jana, S., Leung, M., Chang, J., & Zhang, M. (2014). Effect of nano- and micro-scale topological features on alignment of muscle cells and commitment of myogenic differentiation. *Biofabrication*, *6*(3), 035012.

Järvinen, M. J., & Lehto, M. U. K. (2012). The effects of early mobilisation and immobilisation on the healing process following muscle injuries. *Sports Medicine*, *15*(2), 78–89. https://doi.org/10.2165/00007256-199315020-00002.

Korkut, C., & Budnik, V. (2009). WNTs tune up the neuromuscular junction. *Nature Reviews Neuroscience*, *10*(9), 627–634.

Langhammer, C. G., Kutzing, M. K., Luo, V., Zahn, J. D., & Firestein, B. L. (2013). A topographically modified substrate-embedded MEA for directed myotube formation at electrode contact sites. *Annals of Biomedical Engineering*, *41*(2), 408–420. https://doi.org/10.1007/s10439-012-0647-8.

Langhammer, C. G., Zahn, J. D., & Firestein, B. L. (2010). Identification and quantification of skeletal myotube contraction and association in vitro by video microscopy. *Cytoskeleton*, *67*(7), 413–424. https://doi.org/10.1002/cm.20457.

Lanuza, M. A., Santafe, M. M., Garcia, N., Besalduch, N., Tomàs, M., Obis, T., … Tomàs, J. (2014). Protein kinase C isoforms at the neuromuscular junction: Localization and specific roles in neurotransmission and development. *Journal of Anatomy*, *224*(1), 61–73. https://doi.org/10.1111/joa.12106.

Martin, P. T., & Sanes, J. R. (1997). Integrins mediate adhesion to agrin and modulate agrin signaling. *Development*, *124*(19), 3909–3917.

McClure, M. J., Clark, N. M., Hyzy, S. L., Chalfant, C. E., Olivares-Navarrete, R., Boyan, B. D., & Schwartz, Z. (2016). Role of integrin α7β1 signaling in myoblast differentiation on aligned polydioxanone scaffolds. *Acta Biomaterialia*, *39*, 44–54. https://doi.org/10.1016/j.actbio.2016.04.046.

Menon, K. P., Carrillo, R. A., & Zinn, K. (2013). Development and plasticity of the *Drosophila* larval neuromuscular junction. *Wiley Interdisciplinary Reviews: Developmental Biology*, *2*(5), 647–670.

Piette, J., Bessereau, J.-L., Huchet, M., & Changeux, J.-P. (1990). Two adjacent MyoD1-binding sites regulate expression of the acetylcholine receptor (alpha)-subunit gene. *Nature*, *345*(6273), 353–355.

Ricotti, L., Polini, A., Genchi, G. G., Ciofani, G., Iandolo, D., Vazão, H., … Pisignano, D. (2012). Proliferation and skeletal myotube formation capability of C2C12 and H9c2 cells on isotropic and anisotropic electrospun nanofibrous PHB scaffolds. *Biomedical Materials*, *7*(3), 035010.

Rudnicki, M. A., & Jaenisch, R. (1995). The MyoD family of transcription factors and skeletal myogenesis. *BioEssays*, *17*(3), 203–209. https://doi.org/10.1002/bies.950170306.

Shrirao, A. B., Kung, F. H., Yip, D., Cho, C. H., & Townes-Anderson, E. (2014). Vacuum-assisted fluid flow in microchannels to pattern substrates and cells. *Biofabrication*, *6*(3), 035016.

Shrirao, A. B., Kung, F. H., Yip, D., Firestein, B. L., Cheul, H., & Townes-Anderson, E. (2017). A versatile method of patterning proteins and cells. *JoVE (Journal of Visualized Experiments)*, *120*, e55513.

Smith, C. L., Mittaud, P., Prescott, E. D., Fuhrer, C., & Burden, S. J. (2001). Src, Fyn, and Yes are not required for neuromuscular synapse formation but are necessary for stabilization of agrin-induced clusters of acetylcholine receptors. *The Journal of Neuroscience*, *21*(9), 3151–3160.

Sokolov, P. A., Belousov, M. V., Bondarev, S. A., Zhouravleva, G. A., & Kasyanenko, N. A. (2017). FibrilJ: ImageJ plugin for fibrils' diameter and persistence length determination. *Computer Physics Communications*, *214*, 199–206. https://doi.org/10.1016/j.cpc.2017.01.011.

Tintignac, L. A., Brenner, H.-R., & Rüegg, M. A. (2015). Mechanisms regulating neuromuscular junction development and function and causes of muscle wasting. *Physiological Reviews*, *95*(3), 809–852.

Tourovskaia, A., Kosar, T. F., & Folch, A. (2006). Local induction of acetylcholine receptor clustering in myotube cultures using microfluidic application of agrin. *Biophysical Journal*, *90*(6), 2192–2198. https://doi.org/10.1529/biophysj.105.074864.

Tourovskaia, A., Li, N., & Folch, A. (2008). Localized acetylcholine receptor clustering dynamics in response to microfluidic focal stimulation with agrin. *Biophysical Journal*, *95*(6), 3009–3016.

Trinidad, J. C., Fischbach, G. D., & Cohen, J. B. (2000). The agrin/MuSK signaling pathway is spatially segregated from the neuregulin/ErbB receptor signaling pathway at the neuromuscular junction. *Journal of Neuroscience*, *20*(23), 8762–8770.

Weintraub, H. (1993). The MyoD family and myogenesis: Redundancy, networks, and thresholds. *Cell*, *75*(7), 1241–1244. https://doi.org/10.1016/0092-8674(93)90610-3.

Weston, C. A., Teressa, G., Weeks, B. S., & Prives, J. (2007). Agrin and laminin induce acetylcholine receptor clustering by convergent, Rho GTPase-dependent signaling pathways. *Journal of Cell Science*, *120*(5), 868–875. https://doi.org/10.1242/jcs.03367.

Whitehead, T. J., & Sundararaghavan, H. G. (2014). Electrospinning growth factor releasing microspheres into fibrous scaffolds. *Journal of Visualized Experiments*, *90*. https://doi.org/10.3791/51517.

Yang, H. S., Ieronimakis, N., Tsui, J. H., Kim, H. N., Suh, K.-Y., Reyes, M., & Kim, D.-H. (2014). Nanopatterned muscle cell patches for enhanced myogenesis and dystrophin expression in a mouse model of muscular dystrophy. *Biomaterials*, *35*(5), 1478–1486. https://doi.org/10.1016/j.biomaterials.2013.10.067.

Zhang, D., Sun, M. B., Lee, J., Abdeen, A. A., & Kilian, K. A. (2016). Cell shape and the presentation of adhesion ligands guide smooth muscle myogenesis. *Journal of Biomedical Materials Research Part A*, *104*(5), 1212–1220. https://doi.org/10.1002/jbm.a.35661.

How to cite this article: Kung FH, Sillitti D, Shrirao AB, Shreiber DI, Firestein BL. Collagen nanofibre anisotropy induces myotube differentiation and acetylcholine receptor clustering. *J Tissue Eng Regen Med*. 2018;1–10. https://doi.org/10.1002/term.2632

Appendix 2 - Additional Figures for Chapter 2

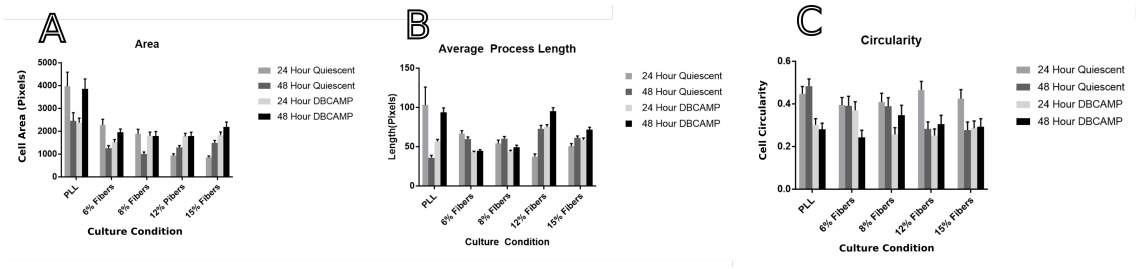

<u>Figure A2.1</u> - Consolidated Graphs of Morphological Markers Measured in Astrocytes. Graphs of complete experimental data for each morphological marker are presented here as the data can be more meaningfully understood as it is presented in Chapter 2. A) Average cell area. B) Average Cell Circularity. C) Average Process Length.

Appendix 3 - Additional Figures for Chapter 3

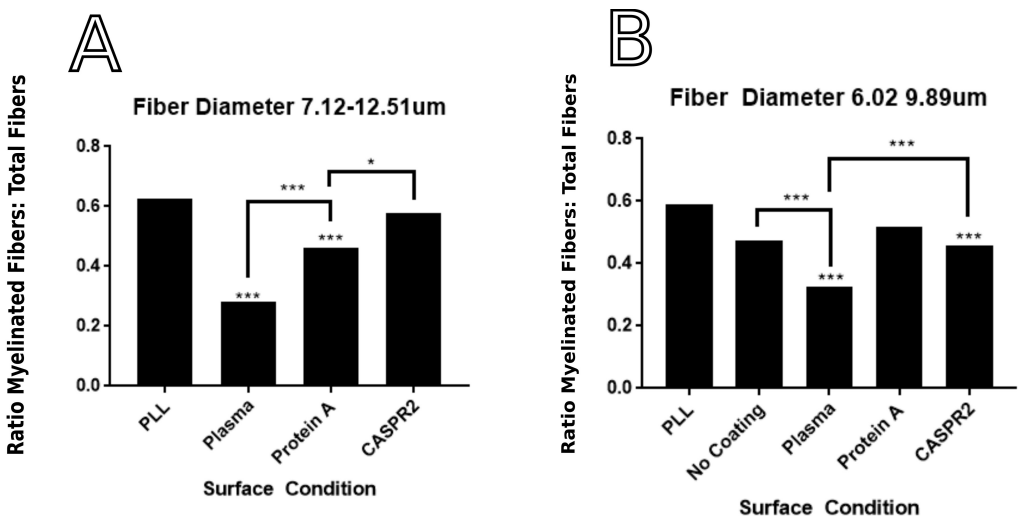

<u>Figure A3.1</u> Graphs of Additional Oligodendrocyte Cultures with Varying Microfiber Diameters. Electrospun PLLA fibers were surface modified as discussed in Chapter 3 Methods. A) Oligodendrocyte and OPC co-culture with microfibers of diameter 7.12 microns to 12.51 microns. Directly adsorped CASPR2 promoted a statistically similar level of interaction as PLL coated fibers, and an increased level of interaction over both other experimental conditions. B) Oligodendrocyte and OPC co-culture with microfibers of diameter 6.02 microns to 9.89 microns. Directly adsorped CASPR2 performed markedly worse than previous cultures, promoting levels of interaction lower than PLL coating, Protein-A coating, and even a non-coated condition. This effect is not observed in other cultures. $p>0.05$ determined by chi square analysis between functionalization conditions.

References

[1] Souzandeh, H., Johnson, K., Wang, Y., Bhamidipaty, K., & Zhong, W. (n.d.). Soy-Protein-Based Nanofabrics for Highly Efficient and Multifunctional Air Filtration. ACS applied materials & interfaces., 8(31), 20023–20031. doi:10.1021/acsami.6b05339

[2] Huang, W., Wang, Y., Chen, C., Law, J., Houghton, M., & Chen, L. (n.d.). Fabrication of flexible self-standing all-cellulose nanofibrous composite membranes for virus removal. Carbohydrate polymers, 143, 9–17. doi:10.1016/j.carbpol.2016.02.011

[3] Nasreen, S., Sundarrajan, S., Nizar, S., Balamurugan, R., & Ramakrishna, S. (n.d.). Advancement in electrospun nanofibrous membranes modification and their application in water treatment. Membranes., 3(4), 266–284. doi:10.3390/membranes3040266

[4] Ren, K., West, J., & Yu, S. (n.d.). Planar microphone based on piezoelectric electrospun poly(γ-benzyl-α,L-glutamate) nanofibers. J Acoust Soc Am, 135(6), EL291–EL297. doi:10.1121/1.4874356

[5] Baniasadi, M., Huang, J., Xu, Z., Moreno, S., Yang, X., Chang, J., Quevedo-Lopez, M., et al. (n.d.). High-performance coils and yarns of polymeric piezoelectric nanofibers. ACS applied materials & interfaces., 7(9), 5358–5366. doi:10.1021/am508812a

[6] Brown, N. (2011). Extracellular matrix in development: insights from mechanisms conserved between invertebrates and vertebrates. Cold Spring Harbor perspectives in biology, 3(12). doi:10.1101/cshperspect.a005082

[7] Feinberg, A., & Parker, K. (n.d.). Surface-initiated assembly of protein nanofabrics. Nano letters., 10(6), 2184–2191. doi:10.1021/nl100998p

[8] Schwarzbauer, J., & Sechler, J. (1999). Fibronectin fibrillogenesis: a paradigm for extracellular matrix assembly. Current opinion in cell biology., 11(5), 622–627.

[9] Pellowe, A., & Gonzalez, A. (n.d.). Extracellular matrix biomimicry for the creation of investigational and therapeutic devices. Wiley interdisciplinary reviews., 8(1), 5–22. doi:10.1002/wnan.1349

[10] Pickup, M., Mouw, J., & Weaver, V. (2014). The extracellular matrix modulates the hallmarks of cancer. EMBO reports, 15(12), 1243–1253. doi:10.15252/embr.201439246

[11] Sechler, J., & Schwarzbauer, J. (1998). Control of cell cycle progression by fibronectin matrix architecture. Journal of biological chemistry., 273(40), 25533–25536.

[12] Leitinger, B., & Hohenester, E. (n.d.). Mammalian collagen receptors. Matrix biology journal of the International Society for Matrix Biology., 26(3), 146–155. doi:10.1016/j.matbio.2006.10.007

[13] Lin, H., Chen, H., Chang, S., & Ni, T. (2013). Pectin-chitosan-PVA nanofibrous scaffold made by electrospinning and its potential use as a skin tissue scaffold. Journal of biomaterials science., 24(4), 470–484. doi:10.1080/09205063.2012.693047

[14] Ho, M., Liao, M., Lin, Y., Lai, C., Lin, P., & Chen, R. (2014). Improving effects of chitosan nanofiber scaffolds on osteoblast proliferation and maturation. International journal of nanomedicine, 9, 4293–4304. doi:10.2147/IJN.S68012

[15] Aitasalo, K., Piitulainen, J., Rekola, J., & Vallittu, P. (n.d.). Craniofacial bone reconstruction with bioactive fiber-reinforced composite implant. Head & neck., 36(5), 722–728. doi:10.1002/hed.23370

[16] Huang, N., Patel, S., Thakar, R., Wu, J., Hsiao, B., Chu, B., Lee, R., et al. (n.d.). Myotube assembly on nanofibrous and micropatterned polymers. Nano letters., 6(3), 537–542. doi:10.1021/nl060060o

[17] Kung, F., Sillitti, D., Shrirao, A., Shreiber, D., & Firestein, B. (n.d.). Collagen nanofibre anisotropy induces myotube differentiation and acetylcholine receptor clustering. Journal of tissue engineering and regenerative medicine, 12(4), e2010–e2019. doi:10.1002/term.2632

[18] Powell, E. M. and Geller, H. M. (1999), Dissection of astrocyte□mediated cues in neuronal guidance and process extension. Glia, 26: 73-83. doi:10.1002/(SICI)1098-1136(199903)26:1<73::AID-GLIA8>3.0.CO;2-S

[19] Gordon, G., Mulligan, S., & MacVicar, B. (n.d.). Astrocyte control of the cerebrovasculature. GLIA., 55(12), 1214–1221. doi:10.1002/glia.20543

[20] Peters, A., Palay, S., Webster, H. *The Fine Structure of the Nervous System.* 3rd ed. New York, NY:Oxford University Press, Inc. 1991

[21] Brown, A., & Ransom, B. (n.d.). Astrocyte glycogen and brain energy metabolism. GLIA., 55(12), 1263–1271. doi:10.1002/glia.20557

[22] Hong, H., Shim, J., Won, Y., Yoo, J., & Hwang, C. (n.d.). Therapeutic time window for the effects of erythropoietin on astrogliosis and neurite outgrowth in an in vitro model of spinal cord injury. Medicine., 97(9), e9913. doi:10.1097/MD.0000000000009913

[23] Anderson, M., Ao, Y., & Sofroniew, M. (n.d.). Heterogeneity of reactive astrocytes. Neuroscience letters., 565, 23–29. doi:10.1016/j.neulet.2013.12.030

[24] Barres, B. (2008). The mystery and magic of glia: a perspective on their roles in health and disease. Neuron., 60(3), 430–440. doi:10.1016/j.neuron.2008.10.013

[25] Bush, T., Puvanachandra, N., Horner, C., Polito, A., Ostenfeld, T., Svendsen, C., Mucke, L., et al. (n.d.). Leukocyte infiltration, neuronal degeneration, and neurite outgrowth after ablation of scar-forming, reactive astrocytes in adult transgenic mice. Neuron., 23(2), 297–308.

[26] Silver, J., & Miller, J. (n.d.). Regeneration beyond the glial scar. Nature reviews., 5(2), 146–156. doi:10.1038/nrn1326

[27] Du, Z., Kolarcik, C., Kozai, T., Luebben, S., Sapp, S., Zheng, X., Nabity, J., et al. (2017). Ultrasoft microwire neural electrodes improve chronic tissue integration. Acta biomaterialia., 53, 46–58. doi:10.1016/j.actbio.2017.02.010

[28] Nicolelis, M., Dimitrov, D., Carmena, J., Crist, R., Lehew, G., Kralik, J., & Wise, S. (n.d.). Chronic, multisite, multielectrode recordings in macaque monkeys. Proceedings of the National Academy of Sciences of the United States of America., 100(19), 11041–11046. doi:10.1073/pnas.1934665100

[29] Chestek, C., Gilja, V., Nuyujukian, P., Foster, J., Fan, J., Kaufman, M., Churchland, M., et al. (n.d.). Long-term stability of neural prosthetic control signals from silicon cortical arrays in rhesus macaque motor cortex. Journal of neural engineering, 8(4), 045005. doi:10.1088/1741-2560/8/4/045005

[30] Min, S., Jung, S., Ju, J., Kwon, Y., Yoon, G., & Shin, H. (2015). Regulation of astrocyte activity via control over stiffness of cellulose acetate electrospun nanofiber. In vitro cellular & developmental biology., 51(9), 933–940. doi:10.1007/s11626-015-9925-8

[31] Tiryaki, V., Ayres, V., Khan, A., Ahmed, I., Shreiber, D., & Meiners, S. (2012). Nanofibrillar scaffolds induce preferential activation of Rho GTPases in cerebral cortical astrocytes. International journal of nanomedicine, 7, 3891–3905. doi:10.2147/IJN.S32681

[32] Tiryaki, V., Ayres, V., Ahmed, I., & Shreiber, D. (n.d.). Differentiation of reactive-like astrocytes cultured on nanofibrillar and comparative culture surfaces. Nanomedicine (Lond), 10(4), 529–545. doi:10.2217/nnm.14.33
[33] Pekny, M., & Pekna, M. (2014). Astrocyte reactivity and reactive astrogliosis: costs and benefits. Physiological reviews., 94(4), 1077–1098. doi:10.1152/physrev.00041.2013
[34] Karussis, D. (n.d.). The diagnosis of multiple sclerosis and the various related demyelinating syndromes: a critical review. Journal of autoimmunity, 48-49, 134–142. doi:10.1016/j.jaut.2014.01.022
[35] Harlow, D., Honce, J., & Miravalle, A. (2015). Remyelination Therapy in Multiple Sclerosis. Frontiers in neurology, 6, 257. doi:10.3389/fneur.2015.00257
[36] Moyon, S., Dubessy, A., Aigrot, M., Trotter, M., Huang, J., Dauphinot, L., Potier, M., et al. (n.d.). Demyelination causes adult CNS progenitors to revert to an immature state and express immune cues that support their migration. The journal of neuroscience : the official journal of the Society for Neuroscience., 35(1), 4–20. doi:10.1523/JNEUROSCI.0849-14.2015
[37] Chari, D., & Blakemore, W. (n.d.). New insights into remyelination failure in multiple sclerosis: implications for glial cell transplantation. Multiple sclerosis., 8(4), 271–277. doi:10.1191/1352458502ms842oa
[38] Rosenberg, S., Kelland, E., Tokar, E., De la Torre, A., & Chan, J. (n.d.). The geometric and spatial constraints of the microenvironment induce oligodendrocyte differentiation. Proceedings of the National Academy of Sciences of the United States of America., 105(38), 14662–14667. doi:10.1073/pnas.0805640105
[39] Sisay, S., Pryce, G., Jackson, S., Tanner, C., Ross, R., Michael, G., Selwood, D., et al. (2013). Genetic background can result in a marked or minimal effect of gene knockout (GPR55 and CB2 receptor) in experimental autoimmune encephalomyelitis models of multiple sclerosis. PloS one., 8(10), e76907. doi:10.1371/journal.pone.0076907
[40] Strauss, K., Puffenberger, E., Huentelman, M., Gottlieb, S., Dobrin, S., Parod, J., Stephan, D., et al. (n.d.). Recessive symptomatic focal epilepsy and mutant contactin-associated protein-like 2. The New England journal of medicine., 354(13), 1370–1377. doi:10.1056/NEJMoa052773
[41] Bullock, P., & Rome, L. (1990). Glass micro-fibers: a model system for study of early events in myelination. Journal of neuroscience research., 27(3), 383–393. doi:10.1002/jnr.490270317
[42] Howe, C. (2006). Coated glass and vicryl microfibers as artificial axons. Cells, tissues, organs., 183(4), 180–194. doi:10.1159/000096509
[43] Lee, S., Leach, M., Redmond, S., Chong, S., Mellon, S., Tuck, S., Feng, Z., et al. (n.d.). A culture system to study oligodendrocyte myelination processes using engineered nanofibers. Nature methods, 9(9), 917–922. doi:10.1038/nmeth.2105
[44] Remahl, S., & Hildebrand, C. (n.d.). Changing relation between onset of myelination and axon diameter range in developing feline white matter. Journal of the neurological sciences., 54(1), 33–45.
[45] Paletta, J., Bockelmann, S., Walz, A., Theisen, C., Wendorff, J., Greiner, A., Fuchs-Winkelmann, S., et al. (n.d.). RGD-functionalisation of PLLA nanofibers by surface coupling using plasma treatment: influence on stem cell differentiation. Journal of materials science., 21(4), 1363–1369. doi:10.1007/s10856-009-3947-
[46] Harrison, R., Steele, J., Chapman, R., Gormley, A., Chow, L., Mahat, M., Podhorska, L., et al. (n.d.). Modular and Versatile Spatial Functionalization of Tissue Engineering Scaffolds through Fiber-Initiated Controlled Radical

Polymerization. Advanced functional materials, 25(36), 5748–5757. doi:10.1002/adfm.201501277

[47] Strauss, K., Puffenberger, E., Huentelman, M., Gottlieb, S., Dobrin, S., Parod, J., Stephan, D., et al. (n.d.). Recessive symptomatic focal epilepsy and mutant contactin-associated protein-like 2. The New England journal of medicine., 354(13), 1370–1377. doi:10.1056/NEJMoa052773

[48] Kastriti, M., Sargiannidou, I., Kleopa, K., & Karagogeos, D. (n.d.). Differential modulation of the juxtaparanodal complex in Multiple Sclerosis. Molecular and cellular neuroscience : MCN., 67, 93–103. doi:10.1016/j.mcn.2015.06.005

[49] Rubio-Marrero, E., Vincelli, G., Jeffries, C., Shaikh, T., Pakos, I., Ranaivoson, F., von Daake, S., et al. (n.d.). Structural Characterization of the Extracellular Domain of CASPR2 and Insights into Its Association with the Novel Ligand Contactin1. Journal of biological chemistry., 291(11), 5788–5802. doi:10.1074/jbc.M115.705681